fluids

MDPI

Article

Heat Transfer Prediction for Internal Flow Condensation in Inclined Tubes

Mateus Henrique Corrêa [1], Victor Gouveia Ferrares [1], Alexandre Garcia Costa [1], Matheus Medeiros Donatoni [2], Maurício Mani Marinheiro [1], Daniel Borba Marchetto [1] and Cristiano Bigonha Tibiriçá [1,*]

[1] Laboratory of Thermal Engineering and Fluid Systems (LETeF), Department of Mechanical Engineering, São Carlos School of Engineering (EESC), University of São Paulo (USP), Av. Trabalhador São-Carlense, 400, São Carlos 13566-590, SP, Brazil
[2] Laboratory of Dynamics, Department of Mechanical Engineering, São Carlos School of Engineering (EESC), University of São Paulo (USP), Av. Trabalhador São-Carlense, 400, São Carlos 13566-590, SP, Brazil
* Correspondence: bigonha@sc.usp.br

Abstract

This study investigates the heat transfer coefficient (HTC) during flow condensation inside smooth inclined tubes, analyzing the combined effects of flow orientation, fluid properties and flow characteristics on the thermal performance. The literature review indicates that the channel inclination effect on the HTC remains insufficiently understood, highlighting the need for further investigation. Thus, a comprehensive experimental database comprising 4944 data points was compiled from 24 studies, including all flow directions, from upward, to horizontal, downward, and intermediate orientations. The study reveals that the influence of flow inclination on the HTC can be ruled by a criterion based on the liquid film thickness Froude number, Fr_δ. At $Fr_\delta > 4.75$, the effect of flow inclination becomes negligible, while under $Fr_\delta < 4.75$, the inclination can have a considerable effect on the HTC. The experimental data show that at low Froude numbers, upward flow typically exhibits higher HTC compared to downward flow, attributed to enhanced interfacial turbulence caused by opposing gravitational and shear forces. In contrast, under vertical downward flow, the annular pattern is more prominent, with reduced interfacial disturbances, limiting HTC performance. The compiled experimental database for inclined channels was compared against an update list of prediction methods, including seven correlations incorporating the inclination angle as an input parameter. Additionally, a new simple correction factor including the effect of inclined tubes was proposed based on the flow inclination angle and on the liquid film thickness Froude number. The proposed correction factor improved the prediction of well-ranked correlations in the literature by over 20% for stratified flow pattern conditions and by more than 5% for low Froude number values. These findings present new insights into how tube inclination can affect heat transfer in a two-phase flow.

Keywords: condensation heat transfer; vertical flow; inclined tubes; heat transfer coefficient; dimensionless correlation; two-phase flow

check for updates

Academic Editors: Moran Wang and Wenning Zhou

Received: 14 October 2025
Revised: 17 November 2025
Accepted: 2 December 2025
Published: 9 December 2025

Citation: Corrêa, M.H.; Ferrares, V.G.; Costa, A.G.; Donatoni, M.M.; Marinheiro, M.M.; Marchetto, D.B.; Tibiriçá, C.B. Heat Transfer Prediction for Internal Flow Condensation in Inclined Tubes. *Fluids* **2025**, *10*, 326. https://doi.org/10.3390/fluids10120326

Copyright: © 2025 by the authors. Licensee MDPI, Basel, Switzerland. This article is an open access article distributed under the terms and conditions of the Creative Commons Attribution (CC BY) license (https://creativecommons.org/licenses/by/4.0/).

1. Introduction

The internal flow condensation process plays a critical role in the design and performance of refrigeration cycles, electrical power plants, heat pumps, desalination plants, and various other thermal systems [1]. Due to the extensive surface area typically required for effective heat rejection, condensers are usually the largest components of these thermal

systems. Given the ongoing efforts to reduce energy consumption and minimize refrigerant charge, the use of compact and high-efficiency heat exchangers has emerged as a key design trend [2]. Accurately predicting the heat transfer coefficient (HTC) during internal flow condensation remains one of the main challenges in the design of efficient condensers, as it is strongly influenced by the complex interplay of multiple parameters. Channel geometry and dimension, as well as the operating conditions (e.g., saturation temperature, mass velocity and vapor quality), have a considerable impact on the HTC. Additionally, the literature highlights that heat transfer performance is also significantly affected by flow orientation [3].

Regarding the flow orientation effect, in certain applications, the condenser inclination is adjusted to optimize thermal performance and minimize occupied volume [1]. For instance, in nuclear power plants, U-tube bundle condensers are typically installed with a downward slope of approximately 3° [1]. In addition, some applications involve variable flow orientations, such as in aircraft during take-off, landing, and banking; automobiles; trucks driving over hilly terrains [4]; and offshore floating power plants, which may become inclined or experience sloshing due to ocean motion [5]. Kharangate et al. [6] also pointed out that most condensers adopt a serpentine design, in which the flow path alternates between vertical downward and upward sections. These scenarios highlight the importance of understanding the effects of flow inclination as a crucial step toward the accurate and reliable prediction of the HTC during condensation.

Despite the increasing use of computational tools including artificial intelligence algorithms, empirical and semi-empirical correlations remain the most practical and widely used approach for HTC prediction in condenser design. These correlations are essential for balancing simplicity and computational efficiency, especially when accounting for varying operating conditions, tube geometries, and fluid properties. In this context, the present study contributes by compiling and analyzing a comprehensive database of HTC experimental results during flow condensation in smooth channels, with particular emphasis on the influence of flow orientation. The main findings support the development of a more accurate predictive correlation, which can serve as a valuable tool for optimizing condenser design.

Flow Orientation Influence on Heat Transfer Coefficient

The main findings in the literature regarding the effect of flow orientation on condensation have been summarized in this section. The analysis encompasses studies conducted in both macro- and micro-scale conditions. Since there is still no consensus regarding the threshold between macro-to-microchannel, Bd $\leq$ 2.86 was adopted in the presented study, following the criterion proposed by Ong and Thome [7]. The present study focuses on HTC data obtained under vertical and inclined flow conditions. However, experimental results for horizontal channels were also considered when obtained during the same experimental campaign of other flow directions, for reference purposes and to minimize potential biases in the analysis.

According to Lips and Meyer [8], an inclination effect on heat transfer during flow condensation was first noticed by Chato [9]. However, growing interest in this research topic has been observed, especially over the past 15 years. Experimental studies have been conducted using a variety of working fluids, including water, hydrocarbons, ammonia, and synthetic refrigerants. A detailed description of the experimental database compiled for the present study is provided in Section 3.

Regarding heat transfer investigations, Lips and Meyer [8] experimentally evaluated the HTC during R134a flow condensation at a T_{sat} of 40 °C and G between 100 and 400 kg/m^{2}s in an 8.38 mm diameter channel under inclinations varying from $-90°$ to 90°.

According to them, the thermal resistance in a condensation process is mainly induced by the heat conduction thermal resistance in the liquid film. Thus, the HTC is strongly dependent on the distribution of the liquid in the tube and, as a consequence, on the flow pattern, which can be influenced by the inclination angle. Based on flow visualization and heat transfer measurements, these authors concluded that the effect of inclination is significant in conditions of low vapor quality (x) and low mass velocity (G), under which different flow topologies are observed depending on the orientation, as shown in Figure 1.

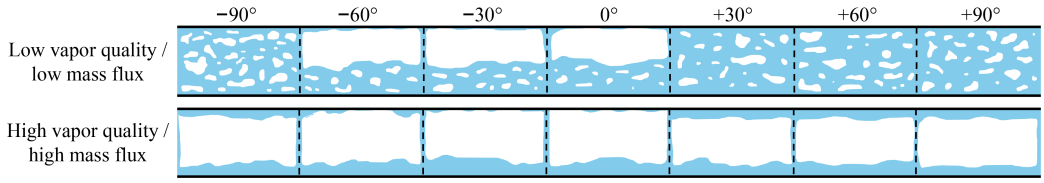


Figure 1. Flow pattern schematic representation of the function of angle, mass flux, and vapor quality. Based on Lips and Meyer [8].

As illustrated in Figure 1, the authors [8] concluded that an increase in vapor quality leads to a progressively more developed annular flow, with reduced sensitivity to variations in inclination. On the other hand, for low vapor qualities, the flow is strongly dependent on the inclination, with wavy stratification for the downward cases (−30° and −60°) and intermittent stratification for the upward cases (+30° and +60°), while both vertical orientations are characterized by turbulence, i.e., churn flow. Similarly, from Figure 1, Lips and Meyer [8] concluded that at a high mass velocity, the flow pattern is annular, independent of inclination, whereas at a low mass velocity, there is a strong dependence of the flow pattern on the tube inclination.

The results reported by Lips and Meyer [8] indicate that increasing the inclination angle from the horizontal position reduces the HTC. This is due to the greater conduction resistance in the liquid film caused by a lower void fraction, as gravitational forces tend to reduce the velocity of the liquid phase. For sharper inclination angles (typically greater than 15° to 30°), flow turbulence is enhanced and the churn flow pattern occurs, leading to a higher HTC compared to the horizontal position, which is induced by the flow instabilities in this pattern. However, reducing the inclination angle from horizontal position led to higher HTCs, which is attributed to the increase in void fraction in downward flow, in which a thinner liquid film is verified. Since the effect of inclination was particularly relevant at low G and x, conditions under which stratified and wavy-stratified flow prevail, downward flow inclinations favor the reduction in liquid film thickness, thereby enhancing the HTC. Such a behavior is maintained up to inclination angles of around −15° to −30°, beyond which the HTC reduces, with the vertical downward orientation exhibiting lower HTCs than those observed under horizontal flow, as seen in Figure 2. The results reported by Lips and Meyer [8] indicate that there is an optimum inclination angle that leads to the highest HTC. Depending on experimental conditions, this optimum inclination angle occurs for downward flow under −15° and −30°. For low vapor qualities, there is also a specific inclination angle (about 15° upward) that leads to the lowest HTC. The conclusions reported by these authors should not be generalized since they mainly tested the fluid R134a, and thermo-physical properties can change considerably from fluid to fluid, leading to different behaviors.

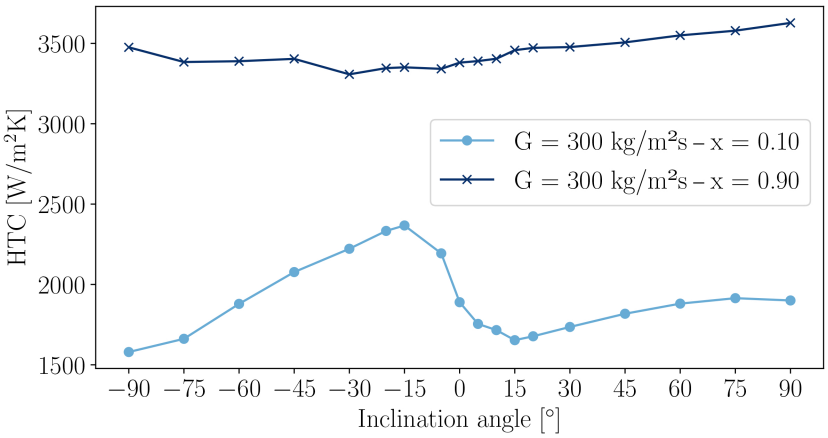


Figure 2. HTC vs. inclination angle. Adapted from Lips and Meyer [8].

Later, Meyer et al. [10] expanded their database for saturation temperatures ranging from 30 to 50 °C. According to the authors, increasing T_{sat} enhances the effect of inclination on the condensing HTC. Such a behavior is attributed to a variation in thermophysical properties with temperature, particularly liquid phase thermal conductivity, which decreases with T_{sat} increment, increasing the liquid film thermal resistance. Ewim et al. [11] reported R134a flow condensation HTC results under smaller mass velocities (50 and 75 kg/m^{2}s). As expected, the more pronounced inclination effect was verified at the lowest mass velocity. In addition, Ewim et al. [11] explored the effect of the temperature difference between the tube surface and the working fluid ($T_w - T_{sat}$) on the heat transfer. According to these authors, the influence of temperature difference on the HTC was more pronounced under downward inclined flow, in which a stratified wavy flow pattern prevails and gravitational effects play a dominant role in the heat transfer process.

Another study with similar characteristics was conducted by Mohseni et al. [12], also using R134a as a working fluid in a smooth tube with a similar inner diameter of 8.38 mm, under various orientations. In this case, the mass velocity ranged from 53 to 212 kg/m^{2}s, and the saturation temperature was 35 °C. For vertical downward flow, the authors observed an annular flow pattern for all mass velocities and vapor qualities, which is attributed to the gravitational force and shear stress acting in the same direction as the flow. The dominance of the annular flow pattern extended to intermediate downward inclinations, such as −60°. For horizontal flow, three distinct flow patterns were observed: annular, wavy-annular, stratified-wavy. For upward orientations, annular flow was observed at high vapor qualities, wavy-annular was identified at intermediate x, churn flow occurred at low vapor qualities and mass velocities, and slug flow appeared at extremely low x and velocities below 148 kg/m^{2}s. It was noted that the influence of flow direction becomes more significant at lower mass velocities, in which gravitational effects are relatively more significant compared to inertial forces. Downward flow yields the lowest HTC due to the flow pattern imposing a thick internal liquid condensate layer around the tube perimeter. Furthermore, since gravitational force and shear stress act in the same direction, no turbulence occurs at the interface. In the upward flow, high interfacial turbulence is observed, leading to higher HTCs at low vapor qualities compared to downward flow. The opposite trend is observed at high vapor qualities, with slightly higher HTCs verified under downward orientations. Figure 3 shows the variation in the heat transfer coefficient (HTC) with inclination angle under extreme vapor quality conditions, according to Mohseni et al. [12]. The light blue curve, corresponding to a low vapor quality, shows a HTC peak at 30°, whereas the darker one, for a high vapor quality, reaches its maximum between −15° and 0°.

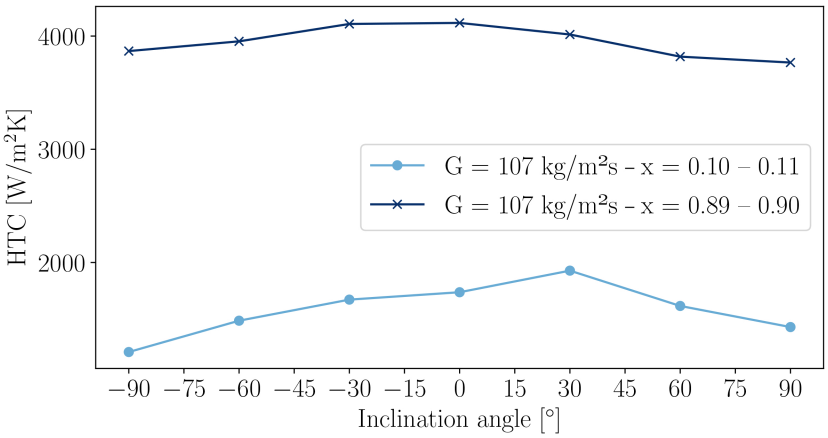


Figure 3. HTC vs. inclination angle. Adapted from Mohseni et al. [12].

The number of experimental studies on vertical and inclined micro-scale condensation is limited, with only a few reporting comprehensive datasets. Among these, the work of Del Col et al. [13] is highlighted, consisting on an experimental investigation of the HTC for R134a and R32 condensation at a T_{sat} of 40 °C inside a square channel with $D_H = 1.23$ mm. Experiments were carried out for horizontal, and 15° to 90° upward and downward flow orientations. According to the authors, the HTCs obtained under horizontal and upward flow conditions were similar for the entire mass velocity range evaluated (100–390 kg/m^{2}s). The influence of channel inclination on HTC became significant only under downward flow at mass velocities lower than 150 kg/m^{2}s for R134a and 200 kg/m^{2}s for R32, conditions in which shear stress effects are less pronounced. Intermediate-to-low vapor quality conditions were also more sensitive to channel inclination effects. It is important to remark that, due to the thicker liquid film, the downflow HTCs measured by these authors were, in general, smaller than those for horizontal flow, and the minimum value occurred under different inclinations depending on G and x. In sum, the results reported by Del Col et al. [13] indicate that, even for a microchannel, gravity still has a role in the distribution of the liquid film along the inner perimeter and, consequently, on the condensation heat transfer process. Interestingly, results for a larger channel diameter ($D = 3.4$ mm), later reported by the same research group [14] under similar experimental conditions, also indicated a similar threshold of $G < 200$ kg/m^{2}s, at which the influence of inclination became significant.

A pattern can be observed in the findings of the authors considered earlier; the HTC is directly related to vapor quality and mass velocity, and depending on the values of these two variables, the orientation can be relevant. At low mass velocities, the flow orientation plays a significant role. For horizontal flow, the trend is seen in liquid film stratification, which affects heat transfer. In downward orientations, the annular flow pattern prevails, typically leading to lower HTCs compared to upward flow. The latter is characterized by opposing forces (shear stress, buoyancy, and gravity) that promote instability at the liquid–vapor interface, enhancing heat transfer. Higher vapor qualities induce an increase in the HTC, as they reduce the liquid film thickness, lowering the thermal resistance in the cross-section.

Thus, it can be summarized that the maximization of the HTC occurs with the increase in mass velocity and vapor quality. When considering low mass velocities, where the flow orientation becomes relevant, the upward flow generally stands out compared to the downward flow.

The majority of flow condensation heat transfer investigations from the literature were carried out in horizontal channels. Therefore, as mentioned in the previous subsection, experimental results obtained under other flow orientations are usually compared against

equivalent data for horizontal conditions. In order to clarify the effect of flow orientation on HTC, experimental results collected from specific datasets selected from the compiled database (described in more detail in Section 3) are graphically presented in this subsection as HTC ratio plots. The following procedure was employed to calculate the HTC ratio: (i) HTC data points under horizontal configuration were collected from HTC vs. vapor quality plots; (ii) HTC data points under other flow orientations were collected from HTC vs. vapor quality plots; (iii) curves corresponding to the experimental data were linearly interpolated without extrapolation to enable direct comparison against similar vapor qualities; (iv) the ratio between non-horizontal and horizontal HTCs for each vapor quality condition was calculated based on the interpolated curves.

A direct comparison between vertical and horizontal flow HTCs was performed for the experimental results reported by Mohseni et al. [12] for a smooth tube with an inner diameter of 8.38 mm. Figure 4 presents the ratios between vertical upward and horizontal HTCs and vertical downward and horizontal HTCs for different mass velocities and vapor qualities. It can be observed from the left and right figures that the HTC ratio progressively approaches 1 as mass velocities increases. Furthermore, for vapor qualities up to approximately 0.65, the upward HTC ratio is greater than that of downward flow. According to the authors, such a behavior may be attributed to the greater interfacial turbulence in upward flows compared to downward flows, which becomes more pronounced at lower vapor qualities.

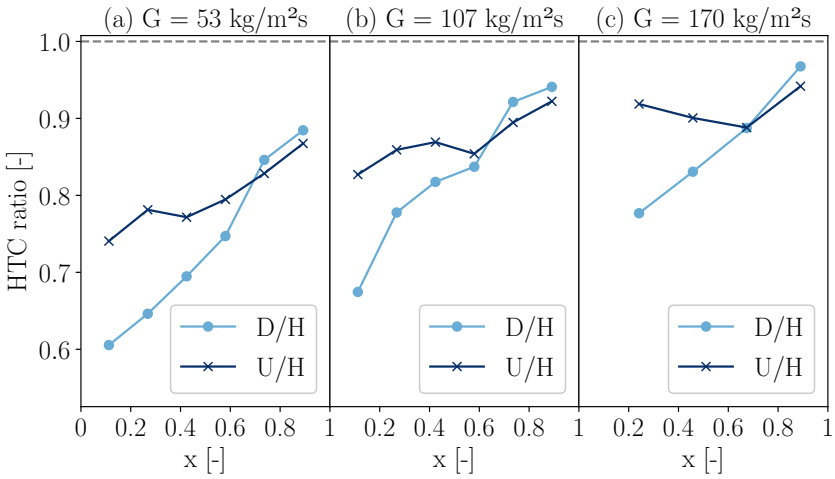


Figure 4. HTC ratio (upward and downward vs. horizontal) for R134a in a smooth tube with a diameter of 8.38 mm. Data extracted from Mohseni et al. [12].

2. Review of Previous Correlations

Due to its critical role in energy, refrigeration, and industrial processes, in-tube flow condensation has been extensively studied, leading to the development of a large amount of HTC prediction methods. An extensive analysis and review of the correlations available in the literature for condensation can be found in the work of Marchetto et al. [15], in which 15021 horizontal and vertical flow condensation HTC datapoints were compared against 34 prediction methods. Among the correlations discussed by the authors, the most traditional or best-performing ones, as well as those that include correction factors based on the inclination angle, are presented in Table 1.

Based on the review conducted by the authors, and further extending the literature survey, a total of 21 correlations were selected for analysis in the present study. These are listed in the Appendix A, Table A1, along with the conditions and working fluids for which they were proposed, as well as their applicability to inclined configurations.

Among the prediction methods summarized in Appendix A, Table A1, 13 of them considered experimental results obtained from vertical and/or inclined channels in their development. However, it should be highlighted that, among these methods, a significant number—Moser et al. [16], Murphy et al. [17], Cavallini and Zecchin [18], Shah [19], Dorao and Fernandino [20,21], Shah [22], Kim and Mudawar [23], and Marinheiro et al. [24]—do not include any explicit parameters that take into account the flow orientation effect in their formulations. In addition, in most cases, non-horizontal flow results correspond only to a small portion of the database gathered by the authors to develop their methods. In practice, inclination effects are either assumed to be negligible or implicitly incorporated into the datasets used to fit correlations, without clear theoretical or experimental justification that would allow generalization over a wide range of angles. Thus, although these methods claim to be applicable to different orientations, such ability, in general, remains insufficiently validated.

Still considering the prediction methods summarized in Appendix A, Table A1, only a small group explicitly considers flow inclination effects, which are usually introduced through correction factors to the horizontal flow HTC. Examples include the correlations proposed by Mohseni et al. [12], Yang et al. [25], Xing et al. [26], Moghadam et al. [27], and Cao et al. [28]. In general, the correlations follow trends experimentally observed or typically reported in the literature, adjusting the HTC as a function of the inclination angle. However, in most cases, the correlations lack physical foundations, such as the influence of liquid phase redistribution, flow pattern transitions, or the balance between gravitational and shear forces. Although these methods are based on experimental observations, and are consistent with the operational ranges investigated, in general, they are limited to representing specific tendencies and do not broadly explore the relationship between inclination and the fundamental mechanisms of flow condensation.

Mohseni et al. [12] developed their correlation based on experimental results for R134a in an 8.38 mm diameter channel under inclinations ranging from −90° to +90°, with 30° angular steps. Based on the prediction method of Boyko and Kruzhilin [29], originally proposed for horizontal flow, Mohseni et al. [12] introduced a correction factor, in which the inclination angle effect is weighted by a function dependent on vapor quality, to incorporate the enhanced effect of flow orientation under low vapor qualities. Yang et al. [25] followed a similar approach, in which the horizontal flow-based method of Akhavan-Behabadi et al. [30] was modified, introducing an inclination-dependent correction factor, in which a cosine function is multiplied by a term dependent on vapor quality. Similarly, the prediction method proposed by Moghadam et al. [27] also incorporates an inclination-dependent multiplying factor to the correlation of Akhavan-Behabadi et al. [30], in which a sine function is used together with a correction based on the vapor quality.

Xing et al. [26] compared R245fa flow condensation HTC data points obtained in a 14.81 mm diameter channel under 13 different inclinations from −90° to +90° with prediction methods from the literature, and verified that the correlation proposed by Shah [31] achieved the lowest deviations for horizontal flow, but showed a loss of accuracy under inclined orientations. Therefore, in the prediction method proposed by Xing et al. [26], the horizontal HTC calculated according to Shah [31] ($h_{\theta=0^\circ}$) is multiplied by a correction factor which includes the flow inclination effect. According to the authors, their prediction method incorporates the general increasing behavior of the HTC with inclination, represented by the term directly dependent on θ, as well as the non-monotonic behavior related to θ, introduced by a sinusoidal term. Cao et al. [28] analyzed the inclined-to-horizontal HTC ratios for R245fa flow condensation in a 14.7 mm diameter channel under $-30^\circ \leq \theta \leq +30^\circ$. According to the authors, the minimum HTC corresponds to $\theta = 0^\circ$, so a factor was included to represent the HTC enhancement due to the inclination. Cao et al. [28] suggest the use

of the correlations proposed by Shah [31] or Dobson and Chato [32] to calculate $h_{\theta=0^\circ}$. Two different empirical parameters (a) were adjusted for $-30^\circ \leq \theta < 0^\circ$ and $0^\circ < \theta \leq +30^\circ$, both including the vapor-phase Froude number, $\mathrm{Fr_v}$, to represent the inertial forces of the vapor, which are expected to reduce the inclination effect on HTC.

Table 1. Evaluated correlations.

Reference	Correlation
Correlations without angular factor	
Shah [19]	$h = h_L\left[(1-x)^{0.8} + \frac{3.8x^{0.76}(1-x)^{0.04}}{p_r^{0.38}}\right]$ Where $h_L = 0.023\mathrm{Re}_{lo}^{0.8}\mathrm{Pr}_l^{0.4}\left(\frac{k_l}{D}\right)$ from the Dittus–Boelter correlation.
Dorao and Fernandino [20]	$h = \left(\frac{k_l}{D}\right)0.023\mathrm{Re}_{2p}^{0.8}\mathrm{Pr}_l^{0.4}$
Dorao and Fernandino [21]	$h = \left(h_I^9 + h_{II}^9\right)^{1/9}$ Where $h_I = \left(\frac{k_l}{D}\right)0.023\mathrm{Re}_{2p}^{0.8}\mathrm{Pr}_{2p}^{0.3}$ $h_{II} = \left(\frac{k_l}{D}\right)41.5D^{0.6}\mathrm{Re}_{2p}^{0.4}\mathrm{Pr}_{2p}^{0.3}$
Marinheiro et al. [24]	$h = \left(\frac{k_l}{D}\right)0.055\mathrm{Re}_{2p}^{0.732}\mathrm{Pr}_{2p}^{0.269}\mathrm{Fr}_l^{-0.091}$
Correlations with angular factor	
Mohseni et al. [12]	$h = \left(\frac{k_l}{D}\right)1.371\mathrm{Pr}^{\frac{1}{3}}\mathrm{Re}_{lo}^{0.69}\left[\frac{\left(\frac{\rho_l}{\rho_m}\right)_{in}^{0.5}+\left(\frac{\rho_l}{\rho_m}\right)_{out}^{0.5}}{2}\right]^{0.91}\left(\frac{\Delta x D}{L}\right)^{0.29}\left(1+(1-x)^{0.1}\cos(\theta-10^\circ)\right)^{0.2}$ Where $\frac{\rho_l}{\rho_m} = 1 + x\left(\frac{\rho_l-\rho_v}{\rho_v}\right)$
Yang et al. [25]	$h = \left(\frac{k_l}{D}\right)A\mathrm{Re}_l^{0.193}\left(\frac{\mathrm{Pr}_l}{\chi_{tt}}\right)^{0.34}F_\alpha^{0.3}$ Where $A = \frac{300D^{0.8}}{\mu_l^{0.145}C_{P,l}^{0.34}k_l^{0.66}}$ $F_\alpha = \frac{1+(1-x)^{0.2}\cos(\theta-10^\circ)}{x^{0.4}}$
Xing et al. [26]	For $0^\circ < \theta < 90^\circ$: $h = h_{\theta=0^\circ}\left(1+\frac{3.024\theta}{\mathrm{Fr}_v^{0.935}}\right)\left[1+\left(\frac{0.172}{\mathrm{Fr}_{lo}^{0.17}x^{0.239}}-0.197\right)\sin(3\theta)\right]$ For $-90^\circ < \theta < 0^\circ$: $h = h_{\theta=0^\circ}\left(1+\frac{3.024\theta}{\mathrm{Fr}_v^{0.935}}\right)\left[1+\left(\frac{0.024}{\mathrm{Fr}_{lo}^{0.584}x^{0.654}}-0.03\right)\lvert\sin(6\theta)\rvert\right]$ Where $h_{\theta=0^\circ}$ is predicted by Shah [31] correlation.
Cao et al. [28]	$h = h_{\theta=0^\circ}(1+a\theta)$ For $0 < \theta \leq \frac{\pi}{6}$: $a = \frac{4.9845}{\mathrm{Fr}_v^{0.3794}} + \frac{36\theta-\pi}{5\pi}\left(\frac{2.4602}{\mathrm{Fr}_v^{0.5162}} - \frac{4.9845}{\mathrm{Fr}_v^{0.3794}}\right)$ For $-\frac{\pi}{6} \leq \theta < 0$: $a = \frac{4.9845}{\mathrm{Fr}_v^{0.3794}} + \frac{36\theta-\pi}{5\pi}\left(\frac{5.0826}{\mathrm{Fr}_v^{0.4067}} - \frac{4.4522}{\mathrm{Fr}_v^{0.5534}}\right)$

Table 1. *Cont.*

Reference	Correlation
Moghadam et al. [27]	$h = \left(\frac{k_l}{D}\right) 4.04 \mathrm{Re}_l^{0.355} \mathrm{Pr}_l^{0.1} \chi_{tt}^{-0.25} F_\theta^{0.7} (1-x)^{-0.14}$ Where $F_\theta = 1 - (1-x)^{0.3} \sin\left(\frac{\theta}{3} - 80^\circ\right)$
Shah [22]	If it is a vertical downward flow, or the fluid is hydrocarbon, or $\mathrm{Re}_l < 100$, then $h = h_{\mathrm{Shah,2013,mod}}$ For horizontal flows, $h_{\mathrm{Shah,2013,mod}} = \begin{cases} h_I & J_v \geq C_1 \quad \text{regime 1} \\ h_{\mathrm{Nu}} & J_v \leq C_2 \quad \text{regime 3} \\ h_I + h_{\mathrm{Nu}} & \text{otherwise} \quad \text{regime 2} \end{cases}$ For vertical flows, $h_{\mathrm{Shah,2013,mod}} = \begin{cases} h_I & J_v \geq C_3 \quad \text{regime 1} \\ h_{\mathrm{Nu}} & J_v \leq C_4 \text{ or } \mathrm{Re}_l < 600 \text{ and } \mathrm{We}_v < 100 \quad \text{regime 3} \\ h_I + h_{\mathrm{Nu}} & \text{otherwise} \quad \text{regime 2} \end{cases}$ If otherwise, $h = h_{\mathrm{Shah,2022}}$ $h_{\mathrm{Shah,2022}} = \begin{cases} h_I & J_v \geq C_1, \mathrm{We}_v > 100 \text{ and } \mathrm{Fr}_l > 0.026 \quad \text{regime 1} \\ h_{\mathrm{Nu}} & J_v \leq C_2 \text{ and } \mathrm{Fr}_l > 0.026 \quad \text{regime 3} \\ h_I + h_{\mathrm{Nu}} & \text{otherwise} \quad \text{regime 2} \end{cases}$ Where $h_I, h_{\mathrm{Nu}}, C_1, C_2, C_3$, and C_4 are defined in Shah [22].

3. Database Description

In the present study, HTC data were compiled from 24 experimental studies on condensation in smooth tubes under vertical, horizontal, and inclined orientations. A total of 4944 data points were digitized using the Engauge Digitizer software (v12.1), and care was taken to exclude duplicate entries. Table 2 summarizes the geometrical characteristics and operational conditions of the collected data.

The database includes vertical, horizontal, and inclined flow configurations. In the present work, the inclination angles reported in the selected studies were standardized as 90° for vertical upward flow and −90° for vertical downward flow, while the remaining angles are between these two vertical orientations. The database encompasses a total of 4833 points (97.75%) distributed according to 13 pure fluids: 4 hydrofluorocarbons (HFCs)—R134a, R32, R245fa, and R236fa; 2 hydrofluoroolefins (HFOs)—R1234yf and R1234ze(E); 2 inorganic fluids—water and ammonia; 2 alkanes—methane and propane; 1 chlorofluorocarbon (CFC)—R113; 1 hydrofluoroether (HFE)—HFE-7100; and 1 fluorocarbon—FC-72. Additionally, three studies reported data for fluid mixtures of methane/ethane (0.828/0.172), methane/ethane (0.590/0.409), and methane/nitrogen (0.837/0.163), totalling 111 data points (2.25%). Figure 5 presents the distribution of data points among the working fluids mentioned.

Table 2. Condensation HTC database description (VU—vertical upward; H—horizontal; VD—vertical downward; I—inclined).

Authors	Fluids	D_h [mm]	p_r [-]	x [-]	HTC [kW/m^{2}K]	G [kg/m^{2}s]	Orientation [VU/H/VD/I]	Data
Brown and Goodykoontz [33]	R113	7.44	0.02–0.08	0.10–0.99	3.00–16.47	831.29–1465.62	0/0/255/0	255
Goodykoontz and Dorsch [34]	Water	7.44	0.00–0.01	0.01–0.96	2.87–124.39	88.34–457.64	0/0/355/0	355
Maråk [35]	Methane Methane[0.590]-Ethane[0.410], Methane[0.828]-Ethane[0.172], Methane[0.837]-Nitrogen[0.163]	0.50–1	0.10–0.91	0.09–0.89	3.56–75.57	160–1360	202/0/0/0	202
Dalkilic et al. [36] *	R134a	8.10	0.25–0.32	0.69–0.98	3.26–12.79	260–515	0/0/64/0	64
Park et al. [37]	R1234ze(E), R134a, R236fa	1.45	0.14–0.44	0.00–0.85	0.73–3.58	100–260	0/0/109/0	109
Del Col et al. [38]	R134a	1.23	0.25	0.20–0.90	1.35–8.72	100–390	58/0/110/0	168
Lips and Meyer [39] *	R134a	8.38	0.25	0.10–0.60	1.00–2.63	50–250	0/10/0/194	204
Lips and Meyer [8] *	R134a	8.38	0.25	0.10–0.90	1.35–4.24	200–600	9/10/10/140	169
Mohseni et al. [12] *	R134a	8.38	0.22	0.10–0.92	0.68–6.09	35–170	17/18/17/72	124
Del Col et al. [13]	R134a, R32	1.23	0.25–0.43	0.19–0.91	1.24–11.98	100–390	39/289/183/677	1188
Meyer et al. [10] *	R134a	8.38	0.19–0.32	0.08–0.89	1.04–4.20	100–400	35/29/35/294	393
Xie et al. [40] *	R245fa	14.81	0.11	0.18–0.64	1.73–3.34	198.30–500.70	19/9/0/0	28
Xing et al. [26] *	R245fa	14.81	0.11	0.11–0.69	1.57–5.04	200–700	23/25/24/0	72
Olivier et al. [41] *	R134a	8.38	0.25	0.10–0.90	1.18–4.38	100–300	12/12/12/192	228
Cao et al. [28] *	R245fa	14.70	0.14	0.16–0.65	2.07–5.83	200–500	0/30/0/112	142
Lin and Wang [42] *	HFE7100	0.80	0.05	0.12–0.87	1.80–5.33	100–300	16/18/16/0	50
Ewim et al. [11] *	R134a	8.38	0.25	0.25–0.75	1.02–2.71	50–300	10/10/10/119	149
Ruzaikin et al. [43] *	Ammonia	8–11	0.12–0.26	0.05–0.80	3.78–16.04	40–160	85/63/57/41	246
Ahn et al. [1]	Water	40	0.00–0.02	0.25–0.96	8.40–14.29	10.05–49.95	0/0/0/19	19
Murphy et al. [17] *	Propane	1.93	0.38–0.66	0.10–0.78	1.11–6.34	75–150	0/0/27/0	27
O'Neill et al. [44]	C6F14	7.12	0.07	0.00–0.97	0.27–8.69	53.80–360.30	112/97/123/0	332
Moghadam et al. [27] *	R1234yf	8.30	0.20	0.12–0.77	1.01–2.82	80–320	31/31/31/124	217
Pusey et al. [45] *	Water	17	0.00	0.26–0.93	7.43–12.76	3.43	0/3/3/18	24
Yang et al. [5] *	Water	25	0.01	0.20–0.85	6.34–18.39	20–50	0/12/0/167	179

* Database refers to the mean vapor quality along the condenser section. The dataset includes 2316 mean vapor quality points and 2628 local vapor quality points.

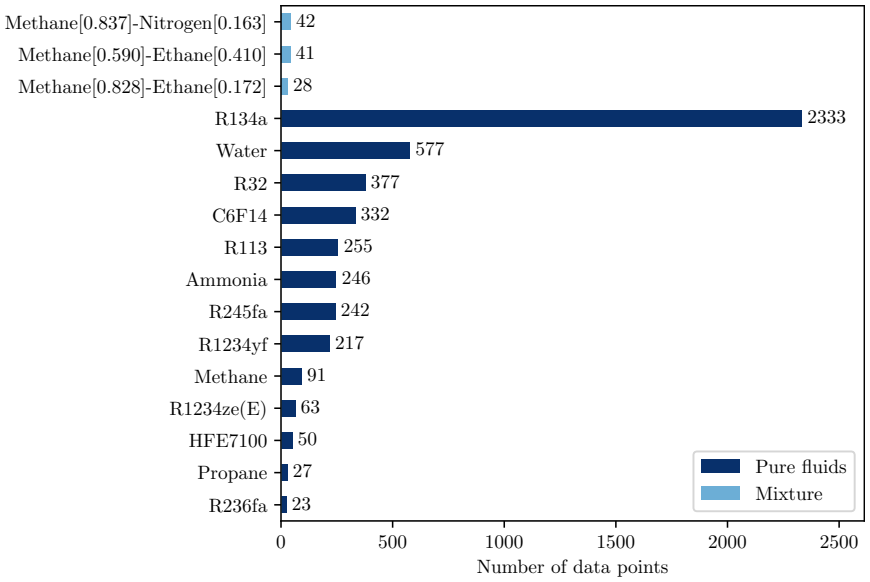
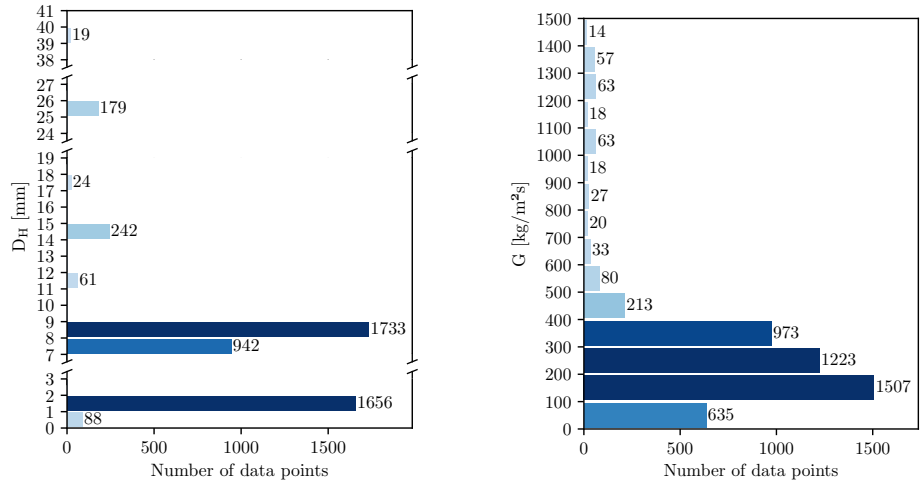


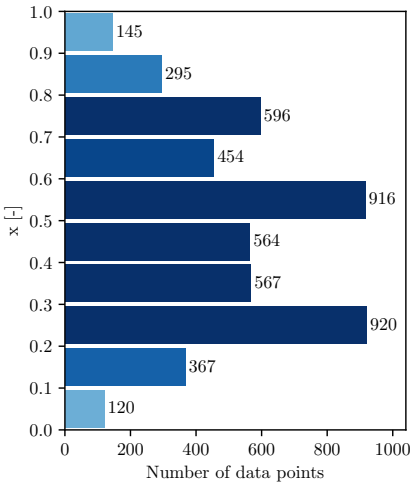
Figure 5. Distribution of the amount of data collected according to the working fluids.

A quantitative analysis of the database was performed, as summarized in Figure 6. Data points are distributed according to five key parameters, as listed in Table 2: hydraulic diameter (D_h, in mm), Figure 6a; mass velocity (G, in kg/m^{2}s), Figure 6b; vapor quality (x), Figure 6c; reduced pressure (p_r), Figure 6d; and angular flow orientation, Figure 6e. The hydraulic diameter analysis, shown in Figure 6a, revealed that 1745 points (35.30%) correspond to micro-channels (Bd $\leq$ 2.86), while 3199 points (64.70%) correspond to conventional channels. Mass velocities varying from 3 to 1465 kg/m^{2}s are shown in Figure 6b, with 92.05% of data corresponding to G < 500 kg/m^{2}s. The database covers the entire vapor quality range 0 < x < 1, as indicated in Figure 6c. Nevertheless, only a small percentage of data points fall within the ranges x < 0.2 and x > 0.8. The reduced pressures distribution, seen in Figure 6d, indicates a concentration of data points at p_r < 0.6. Considering the data distribution according to the flow direction, seen in Figure 6e, 29.15% (1441 data points) correspond to vertical downward flow, 13.51% (668 data points) to vertical upward flow, and 13.47% (666 data points) to horizontal flow. The remaining 43.87% (2169 data points) correspond to inclined flow orientations.

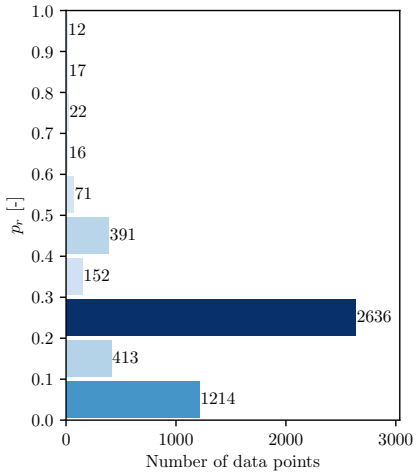


(**a**) Hydraulic diameter. (**b**) Mass velocity.

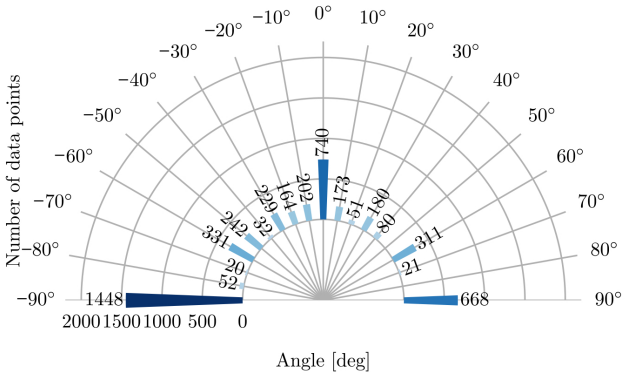
Figure 6. *Cont*.



(**c**) Vapor quality.



(**d**) Reduced pressure.



(**e**) Flow angle.

Figure 6. Data points distribution.

The database covers five flow patterns, classified according to El Hajal et al. [46], with most experimental results corresponding to annular, intermittent, and especially stratified-wavy patterns. The flow pattern map of El Hajal et al. [46] was chosen due to its well-established use in the literature [22,27]. Figure 7 presents the histogram of flow patterns.

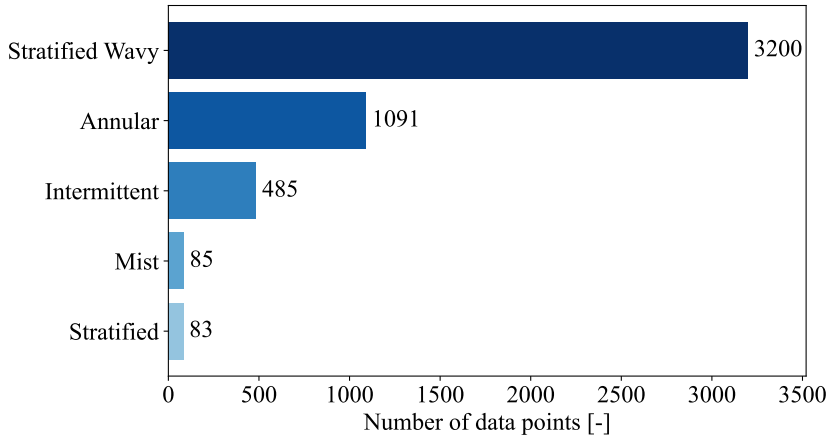


Figure 7. Flow pattern histogram for the database.

4. Development of Correlation for Inclined Tubes

This section presents the development of a criterion for identifying experimental conditions in which flow orientation has a relevant influence. Then, a simple correlation is proposed to correct the HTC from horizontal flow to other orientations, which is based on the channel inclination angle and the Froude number.

4.1. Criterion for Including the Effect of Inclination Angle on Internal Flow Condensation Heat Transfer

The basis for the development of a correlation for predicting the HTC during flow condensation inside inclined channels first requires the establishment of a criterion to identify the conditions under which tube inclination affects the heat transfer process. As discussed in the literature review, channel inclination exerts only a minor influence on the HTC at high flow velocities. Heat transfer during flow condensation is strongly governed by liquid film thickness. Therefore, introducing a criterion sensitive to film thickness variations is a promising approach to assess the relative effects of inclination angle.

Schubring and Shedd [47] developed a model for the liquid film thickness asymmetry in horizontal flows, which is replicated below:

$$\delta_{t,b} = \frac{\delta_t}{\delta_b} = 1 - \exp\left(-0.63\mathrm{Fr}_\delta\right) \tag{1}$$

where

$$\mathrm{Fr}_\delta = \frac{Gx}{\rho_l (9.81\delta_m)^{0.5}} \tag{2}$$

$$\delta_m = \frac{4.7D}{x}\left(\frac{\rho_v}{\rho_l}\right)^{1/3} \mathrm{Re}_{lo}^{-2/3} \tag{3}$$

$$\mathrm{Re}_{lo} = \frac{GD}{\mu_l} \tag{4}$$

where $\delta_{t,b}$ is the top-to-bottom liquid film thickness ratio, Fr_δ is the Froude number based on the liquid film thickness, δ_m is the circumferentially averaged base film thickness, and Re_{lo} is the Reynolds number assuming the entire flow as liquid.

Numerous relations between HTC and liquid film thickness have been developed throughout the literature for different flow and boundary conditions [48]. One of the classical formulations is the Nusselt laminar condensation film theory, which gives

$$h = \frac{k_l}{\delta} \tag{5}$$

where h is local HTC, k_l is the liquid thermal conductivity, and δ is the local liquid film thickness.

Thus, according to Equation (5), if the channel inclination affects the liquid film thickness along the tube perimeter, the HTC should also be affected.

Assuming that a $\delta_{t,b} = 0.95$ represents a condition in which liquid film asymmetry has a negligible effect on the circumferentially averaged HTC, a criterion for identifying the influence of inclination angle can be defined. For illustration, consider a bottom film thickness of 1 mm. If $\delta_{t,b} = 0.95$, the average film thickness along the tube perimeter can be roughly approximated as 0.975, and the change in HTC can be evaluated by $h = k_l/\delta = k_l/0.975 = 1.026k_l$, which is below 5%. The liquid film thickness Froude number, Equation (1), associated with $\delta_{t,b} = 0.95$ is $\mathrm{Fr}_\delta = 4.75$. Therefore, the following criterion is established:

$$\mathrm{Fr}_\delta > 4.75 \;\rightarrow\; \text{gravity forces are negligible} \tag{6}$$

For Fr_δ values higher than 4.75, the asymmetry in liquid film thickness results in only a small change in the circumferentially averaged HTC. The exact magnitude of this change will be determined in the following section by the data regression of Table 2. This criterion reflects the balance between gravitational and inertial forces. At higher Fr_δ, gravity is no longer able to stratify the liquid film and induce asymmetry. As a result, the impact of gravity forces, and thus of the inclination angle, on the HTC becomes negligible.

4.2. New Correlation Including the Effect of Inclination Angle on Internal Flow

Since the film thickness Froude number is relevant for determining the influence of gravity forces on two-phase flow in inclined channels, it is natural to include this dimensionless number in a correlation. Furthermore, the database described in Section 3 indicates a general trend of increasing HTC with increasing inclination angle. Such behavior is conditioned by the Froude number. Figure 8 illustrates the typical effects of the inclination angle on the HTC under different Froude numbers, based on the experimental results reported by the studies summarized in Table 2.

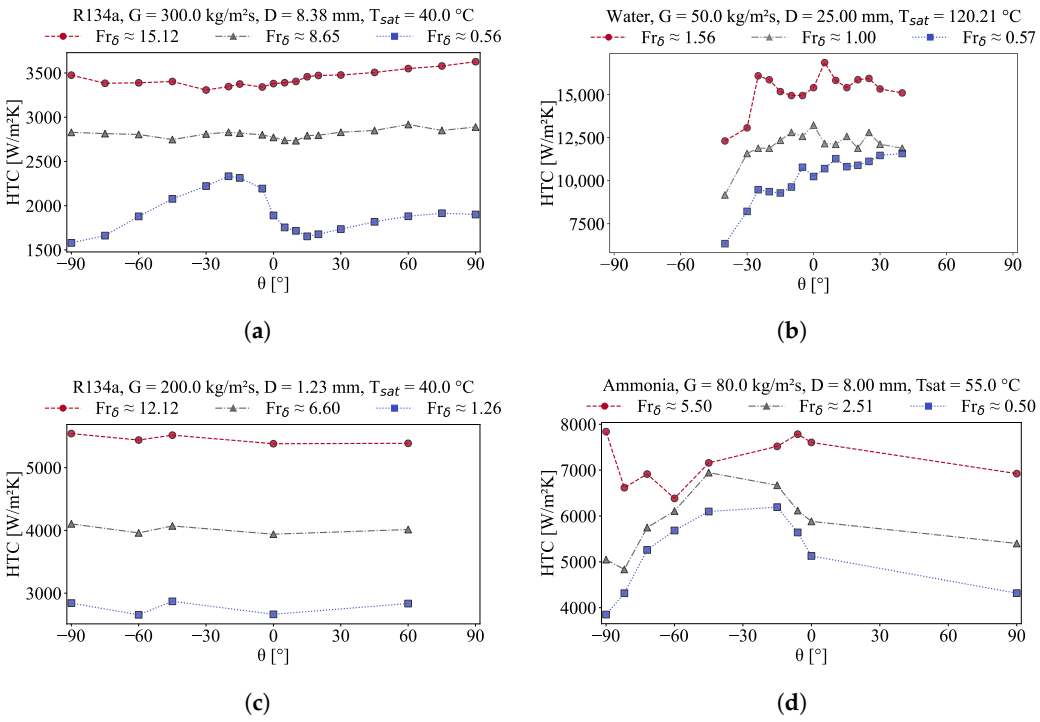


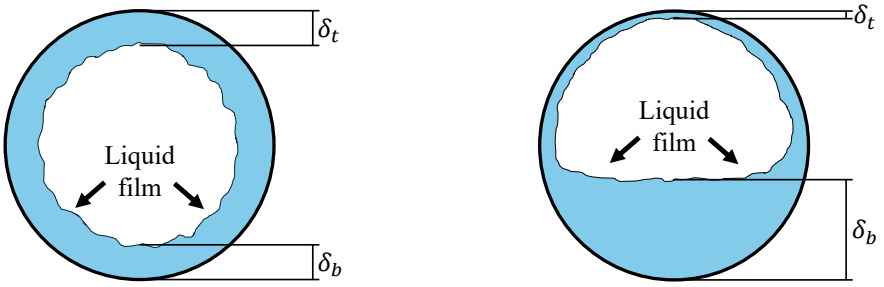
Figure 8. Parametric effect of tube inclination for different levels of Froude number. (**a**) Data from Lips and Meyer [8]. (**b**) Data from Yang et al. [5]. (**c**) Data from Del Col et al. [13,38]. (**d**) Data from Ruzaikin et al. [43].

For higher Fr_δ (typically > 4.75), a low influence of inclination angle is clearly observed. For lower Fr_δ, the HTC tends to exhibit a peak near the horizontal orientation. This behavior is associated with the maximized liquid film asymmetry around the tube perimeter for near horizontal flows, which results in higher circumferentially averaged HTCs. Since the HTC is usually considered inversely proportional to the liquid film thickness (please see Equation (5)), integrating the liquid film thickness along the perimeter yields higher HTCs for asymmetric films than for symmetric distributions, considering a given void fraction, as illustrated in Figure 9.

Considering the above-outlined aspects, the following procedure is proposed for accounting the effect of inclination angle. Firstly, a correlation that accurately predicts the HTC for Fr_δ > 4.75 should be established. Then a correction factor, F, can be applied to this correlation to account for the influence of inclination when Fr_δ < 4.75.

Thus, based on the database of Marchetto et al. [15] a total of 9512 experimental points were obtained for $Fr_\delta > 4.75$. A correlation similar to Marinheiro et al. [24] was adjusted to this data bank and is written below:

$$Nu_{2p} = \frac{h_{2p}D}{k_l} = 0.0279 Re_{2p}^{0.8} Pr_{2p}^{0.2} Fr_{lo}^{-0.069} \quad \text{for } Fr_\delta > 4.75 \tag{7}$$



(**a**) Symmetric distribution. (**b**) Asymmetric distribution.

Figure 9. Representation of liquid film distribution.

The coefficients of this correlation are similar to the Dittus and Boelter [49] equation, reinforcing turbulent characteristics for conditions of $Fr_\delta > 4.75$. Equation (7) obtained similar predictions of the original Marinheiro et al. [24] correlation for the database of Marchetto et al. [15] for $Fr_\delta > 4.75$ (22.6% vs. 23.1% MAPE, respectively). It should be mentioned that the database used for the development of Marinheiro et al. [24] has almost 70% of the data points with $Fr_\delta > 4.75$.

The next step is the development of a correction factor, $F(\theta, Fr_\delta)$, as a function of inclination angle and Fr_δ, for conditions of $Fr_\delta < 4.75$, in which inclination affects the HTC. To adjust this correction factor correlation, the database for inclined channels compiled in the current work, Table 2, was used. Initially, a fifth-order polynomial equation was tested to capture the functional dependence on inclination angle. After extensive testing and refinement, including the evaluation of sine, tanh, exp, and power-law expressions, the final correlation, Equation (8), was selected. It features a parabolic dependence on inclination angle and incorporates the influence of Fr_δ.

$$F(\theta, Fr_\delta) = \left[1 + \frac{1.135 + 1.56 \cdot 10^{-3}\theta - 1.074 \cdot 10^{-4}\theta^2}{0.644 + \left(\frac{Fr_\delta}{0.444}\right)^{1.321}}\right] \tag{8}$$

In Equation (8), θ is the inclination angle in degrees, and it should be kept in the range between $-90°$ to $+90°$ ($\theta = 0°$ = horizontal; $\theta = -90°$ = vertical downward; $\theta = +90°$ = vertical upward), and Fr_δ is calculated according to Equation (2). The coefficients of Equation (8) were adjusted using the least-squares method based on the comparison between the experimental data summarized in Table 2 and the product of Equations (7) and (8). Linear regression, the generalized reduced gradient method, and the Nelder–Mead simplex algorithm were employed during data regression [24]. Fluid properties should be evaluated at a saturated state.

As illustrated in Figure 10, for the proposed correlation, Equation (8), F approaches 1 when Fr_δ approaches 4.75. For $\theta = 0°$ and $Fr_\delta < 4.75$, the correlation yields values higher than 1, capturing the effect of liquid film asymmetry, which increases the circumferentially averaged HTC. For $\theta = 0°$ and $Fr_\delta = 4.75$, the value F = 1.048, reflecting the small influence of the inclination correction factor for $Fr_\delta > 4.75$. The parabolic dependence on the inclination angle results from the regression of the experimental data, which shows a peak at slightly positive inclination angles. The higher values for upward flow can be related

to the additional gas velocity component induced by buoyancy, compared the downward flow condition.

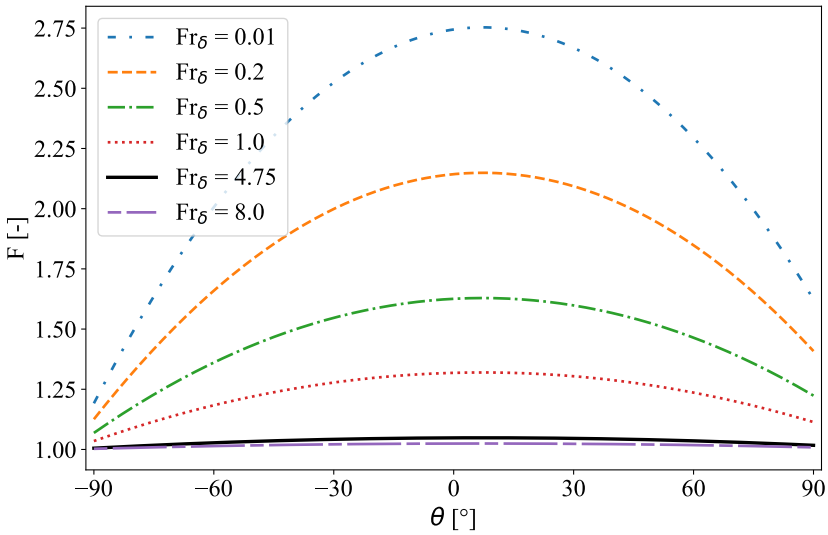


Figure 10. Correction factor F(θ) as function of film thickness Froude number.

The final HTC is obtained by multiplying the correction factor, F(θ, Fr$_\delta$), to a correlation that was adjusted mainly with data of Fr$_\delta$ > 4.75 and has a single flow regime. From the correlations discussed on Table 1, three of them are prone to use the correction factor, since they have no regime distinction for low and high flow velocities. These are the correlations of Shah [19], Dorao and Fernandino [20] and Marinheiro et al. [24]. Thus, the correction factor can be applied for the calculation of the HTC in straight tubes under any inclination angle and Froude number for internal flow condensation, as indicated in Equation (9).

$$\mathrm{HTC}(\theta) = \mathrm{F}(\theta, \mathrm{Fr}_\delta) \times \mathrm{HTC}_{\mathrm{Fr}_\delta > 4.75} \tag{9}$$

where HTC$_{\mathrm{Fr}_\delta > 4.75}$ should be a correlation with only one flow regime suitable for Fr$_\delta$ > 4.75, with no inclination angle dependence, and F(θ, Fr$_\delta$) is given by Equation (8).

5. Comparative Evaluation of the Proposed Correlation

Table 3 compares the predictions of correlations in the literature against the current database for inclined tubes. The criteria used for evaluation were the MAPE, $\lambda_{30\%}$, and $\lambda_{50\%}$. The gray shaded cells are the correlations corrected by the angle factor, F, as described in Equation (8). The blue cells are correlations that account for the inclination angle in their original version. The remaining cells are the correlations without angle as the input parameter. It can be observed that for the four gray shaded correlations, the error was consistently reduced when compared to the correlations without the correction factor F. In this table, the data are also analyzed separately for both macro- and mini-channels, following the transition threshold of Ong and Thome [7]. The correlations corrected by the factor F showed enhanced predictive accuracy for both macro- and mini-channels. For macro-channel data, a higher improvement is noted, corroborating the suggestion that in mini-channels, the gravity force effects are less pronounced. The improvements achieved by the correction factor F remained close to 3–4%, depending on the correlation. The lowest MAPE was obtained by the prediction method of Marinheiro et al. [24] multiplied by the correction factor F, exhibiting an MAPE of 24.1%. Equation (7) × F showed a slightly higher MAPE than Marinheiro et al. [24] × F, a result that can be attributed to the larger database used by Marinheiro et al. [24] to adjust their correlation, which includes more

than 12,000 points and 69 different fluids, reinforcing the importance of a comprehensive data bank for adjusting correlations. The correlation of Moradkhani et al. [50] was also evaluated in this work, but for 17 specific datapoints, it returned extremely high HTC values, resulting in an MAPE above 100% for the complete database analysis.

Table 3. Comparison of predictive methods for the database in Table 2: the whole database, macro-channel, and mini-channel points.

Methods/Databases	All Database (4944 Points)			Macro-Channel (3199 Points)			Mini-Channel (1745 Points)		
	MAPE [%]	$\lambda_{30\%}$ [%]	$\lambda_{50\%}$ [%]	MAPE [%]	$\lambda_{30\%}$ [%]	$\lambda_{50\%}$ [%]	MAPE [%]	$\lambda_{30\%}$ [%]	$\lambda_{50\%}$ [%]
Akers et al. [51]	58.2	39.4	58.7	30.4	56.0	80.6	109.2	8.8	18.6
Traviss et al. [52]	39.7	53.7	77.4	39.0	47.3	74.1	40.9	65.3	83.7
Cavallini and Zecchin [18]	32.4	59.9	85.2	30.0	56.8	86.7	36.7	65.7	82.3
Shah [19]	28.1	62.1	84.3	28.2	60.0	86.0	28.0	66.0	81.4
Shah [19] × F *	25.0	70.2	89.2	**24.3**	**70.4**	**92.0**	26.3	69.8	84.2
Moser et al. [16]	32.2	62.3	82.7	30.9	61.5	82.0	34.5	63.9	84.1
Chang et al. [53]	33.6	46.0	78.6	33.1	48.0	77.6	34.6	42.5	80.3
Moser et al. [16] modified ***	49.7	39.0	72.0	56.8	41.4	67.3	36.8	34.7	80.5
Bohdal et al. [54]	75.8	25.5	44.2	54.6	33.2	57.5	114.7	11.4	19.8
Kim and Mudawar [23]	33.8	53.3	81.9	34.0	47.1	79.9	33.5	64.6	85.6
Mohseni et al. [12] **	92.9	30.8	44.2	119.6	16.4	24.1	44.1	57.1	80.9
Yang et al. [25] **	53.6	20.7	40.8	49.5	29.4	54.1	61.0	4.6	16.4
Xing et al. [26] **	50.4	63.1	83.4	47.2	63.5	83.2	56.5	62.5	84.0
Macdonald and Garimella [55]	80.3	29.2	55.6	94.4	32.3	58.4	54.6	23.6	50.5
Cao et al. [28] **	33.0	59.9	81.8	37.3	56.5	79.4	25.0	66.1	86.1
Dorao and Fernandino [20]	33.2	49.6	75.4	35.0	46.8	70.0	29.9	54.7	85.3
Dorao and Fernandino [20] × F *	29.1	59.3	80.4	30.2	56.5	76.8	27.2	64.4	87.0
Dorao and Fernandino [21]	26.1	65.9	87.4	25.2	68.1	87.6	27.7	61.9	87.0
Murphy et al. [17]	68.3	33.8	53.6	77.2	22.5	41.5	51.9	54.4	75.9
Hosseini et al. [56]	29.9	55.8	87.7	27.5	65.7	90.4	34.4	37.7	82.9
Moghadam et al. [27] **	56.5	35.5	53.9	36.9	45.8	68.0	92.4	16.4	28.0
Shah [22] **	25.4	70.2	89.3	24.8	68.3	91.5	26.7	73.5	85.1
Nie et al. [57]	26.2	66.0	86.7	25.3	66.1	86.2	28.0	65.8	87.5
Marinheiro et al. [24]	26.9	64.3	86.0	28.8	57.3	83.0	23.2	77.1	91.6
Marinheiro et al. [24] × F *	**24.1**	**71.9**	89.9	25.6	68.6	88.2	**21.3**	**78.0**	**93.0**
Equation (7)	28.9	59.6	84.4	30.1	55.8	82.0	26.7	66.6	88.7
Equation (7) × F *	25.4	69.0	**90.1**	26.0	65.3	90.1	24.2	75.8	90.0

* These correlations, shaded in gray, have just one flow regime and have been corrected by angle factor, Equations (8), and (9). ** The blue shaded cells are correlations which account for the flow inclination angle. *** Moser et al. [16], with the Zhang and Webb [58] pressure drop model. The best-performed MAPE, λ_{30} and λ_{50} for each group is in bold and underlined.

In order to verify the criterion established by Equation (6), which assumes that if $Fr_\delta < 4.75$, the inclination effects are relevant, the database summarized in Table 2 was divided into two subsets: $Fr_\delta < 4.75$ and $Fr_\delta > 4.75$, as presented in Table 4. For the gray shaded rows, where the correction factor F was applied, a clear improvement in prediction accuracy is observed for the $Fr_\delta < 4.75$ group, with MAPE reductions between 4 and 6%. In contrast, for $Fr_\delta > 4.75$ the MAPE remained nearly unchanged when using the corrected correlations, as F tends to 1 as Fr_δ approaches 4.75.

Table 4. Comparison of predictive methods for the database on Table 2, with data divided into $Fr_\delta > 4.75$ (no inclination angle effect) and $Fr_\delta < 4.75$ groups.

Methods/Databases	$Fr_\delta < 4.75$ (2841 Points)			$Fr_\delta > 4.75$ (2103 Points)		
	MAPE [%]	$\lambda_{30\%}$ [%]	$\lambda_{50\%}$ [%]	MAPE [%]	$\lambda_{30\%}$ [%]	$\lambda_{50\%}$ [%]
Akers et al. [51]	60.2	44.1	62.8	55.4	33.0	53.2
Traviss et al. [52]	30.9	57.9	84.3	51.5	47.9	68.1
Cavallini and Zecchin [18]	28.9	60.6	85.6	37.0	59.0	84.6
Shah [19]	29.8	55.5	82.5	25.9	70.9	86.8
Shah [19] × F *	24.1	70.6	90.8	26.3	69.6	87.0
Moser et al. [16]	32.1	57.4	81.2	32.2	68.9	84.9
Chang et al. [53]	37.8	37.2	73.3	28.1	58.0	85.7
Moser et al. [16] modified ***	55.3	31.5	67.5	42.2	49.2	78.0
Bohdal et al. [54]	79.2	27.8	47.2	71.2	22.4	40.2
Kim and Mudawar [23]	34.5	46.5	79.7	32.9	62.4	85.0
Mohseni et al. [12] **	94.7	31.2	43.0	90.6	30.2	45.7
Yang et al. [25] **	49.3	24.4	50.0	59.4	15.7	28.4
Xing et al. [26] **	70.0	56.2	78.5	**24.0**	72.5	90.1
Macdonald and Garimella [55]	50.5	31.2	63.1	120.7	26.6	45.5
Cao et al. [28] **	37.2	55.6	79.3	27.2	65.6	85.1
Dorao and Fernandino [20]	38.6	36.9	69.7	25.9	66.9	83.1
Dorao and Fernandino [20] × F *	31.7	53.0	78.1	25.7	67.9	83.6
Dorao and Fernandino [21]	26.2	64.4	89.3	25.9	68.0	84.9
Murphy et al. [17]	51.9	36.1	62.4	90.3	30.6	41.7
Hosseini et al. [56]	31.6	54.5	87.8	27.7	57.7	87.6
Moghadam et al. [27] **	56.6	40.1	58.6	56.3	29.2	47.5
Shah [22] **	25.2	66.4	88.3	25.7	**75.3**	**90.5**
Nie et al. [57]	24.6	69.8	88.6	28.4	60.8	84.1
Marinheiro et al. [24]	27.6	61.8	85.9	25.9	67.6	86.3
Marinheiro et al. [24] × F *	**22.8**	**74.8**	**92.1**	25.9	68.0	87.0
Equation (7)	30.9	52.9	80.7	26.2	68.7	89.3
Equation (7) × F *	24.7	70.3	90.5	26.4	67.2	89.5

* These correlations, shaded in gray, have just one flow regime and have been corrected by angle factor, Equations (8) and (9). ** The blue shaded cells are correlations which account for the flow inclination angle. *** Moser et al. [16], with the Zhang and Webb [58] pressure drop model. The best-performed MAPE, λ_{30} and λ_{50} for each group is in bold and underlined.

Table 5 compares the data for vertical upward, downward, and horizontal flow conditions. As well as for the analysis presented in Tables 3 and 4, a consistent improvement is observed for all correlations corrected by the F factor, Equation (8). Approximately half of the data correspond to vertical downward flow, and interestingly, the correlation of Shah [19] multiplied by the correction factor F exhibited the lowest MAPE, 22.5%, for this flow direction. For vertical upward flow, the lowest MAPE was obtained by the correlation of Marinheiro et al. [24] multiplied by the correction factor F. Under horizontal conditions, the correlation of Shah [22] resulted in an MAPE of 17.1%.

Table 6 presents a statistical analysis of the comparisons, considering the database divided by flow patterns according to the flow pattern map of El Hajal et al. [46]. It should be remarked that this map was originally developed for horizontal flow, and the classification used here is only indicative. According to this table, the data reported as stratified flow exhibited the highest errors among the flow patterns, but also the largest

improvements due to the correction factor F, corresponding to around a 20% reduction in the MAPE. Stratified flow patterns are typically characterized by low gas and liquid velocities. Under these conditions, gravitational forces are more relevant, resulting in lower Fr_δ numbers, and higher correction factor F, which corresponds to greater liquid film asymmetry. Moreover, an ideal stratified flow, with gas on the top and liquid on the bottom, is less likely to occur during condensation due to the mechanism of droplet and film condensation that keeps the entire surface wetted, affecting the overall circumferential HTC. For annular and mist flows, the improvement provided by the correction factor was smaller, since the Froude number under these conditions approaches 4.75.

Table 5. Comparison of predictive methods for the database in Table 2, subdivided by horizontal, upward, and downward tube flow directions.

Methods/Databases	Horizontal (666 Points)			Upward (1558 Points)			Downward (2720 Points)		
	MAPE [%]	$\lambda_{30\%}$ [%]	$\lambda_{50\%}$ [%]	**MAPE** [%]	$\lambda_{30\%}$ [%]	$\lambda_{50\%}$ [%]	**MAPE** [%]	$\lambda_{30\%}$ [%]	$\lambda_{50\%}$ [%]
Akers et al. [51]	61.3	27.9	46.5	50.2	47.1	64.1	62.0	37.8	58.6
Traviss et al. [52]	25.3	64.0	89.9	50.4	45.5	74.5	37.1	55.8	76.1
Cavallini and Zecchin [18]	23.2	67.9	93.5	43.4	52.5	77.8	28.3	62.2	87.4
Shah [19]	23.4	67.9	91.7	34.6	52.9	74.9	25.6	66.0	87.9
Shah [19] × F *	21.7	76.9	93.2	30.7	63.5	81.9	**22.5**	**72.4**	**92.4**
Moser et al. [16]	24.4	67.9	89.2	37.4	59.1	77.2	31.1	62.9	84.3
Chang et al. [53]	33.4	44.4	81.4	36.2	41.1	71.6	32.3	49.2	81.9
Moser et al. [16] modified ***	35.3	35.7	79.9	34.7	45.8	73.7	61.8	36.0	69.0
Bohdal et al. [54]	84.0	15.6	27.3	58.6	36.4	56.8	83.7	21.7	41.1
Kim and Mudawar [23]	28.9	58.3	89.6	38.8	50.5	76.6	32.2	53.7	83.1
Mohseni et al. [12] **	76.2	35.1	54.4	94.6	27.3	41.0	96.1	31.7	43.5
Yang et al. [25] **	51.3	18.3	40.8	49.1	28.0	47.4	56.7	17.1	37.0
Xing et al. [26] **	21.6	68.5	96.2	37.2	59.9	79.5	65.1	63.7	82.5
Macdonald and Garimella [55]	38.4	30.2	73.0	55.1	33.9	59.2	105.0	26.4	49.3
Cao et al. [28] **	21.6	68.5	96.2	43.7	50.3	70.9	29.6	63.2	84.4
Dorao and Fernandino [20]	29.9	51.5	86.2	33.4	49.5	72.5	33.8	49.2	74.4
Dorao and Fernandino [20] × F *	25.7	66.2	91.1	28.6	60.4	78.4	30.2	57.0	79.0
Dorao and Fernandino [21]	25.4	64.3	92.5	26.0	66.5	85.5	26.3	66.0	87.2
Murphy et al. [17]	47.4	40.5	67.3	83.2	26.0	45.7	64.8	36.5	54.8
Hosseini et al. [56]	30.3	47.7	92.3	28.5	57.4	85.2	30.7	56.9	88.1
Moghadam et al. [27] **	58.7	26.0	44.4	46.8	45.4	63.2	61.4	32.1	50.9
Shah [22] **	**17.1**	**84.4**	**96.4**	31.5	64.5	83.4	24.0	69.9	90.9
Nie et al. [57]	23.7	69.4	95.9	25.1	68.9	87.0	27.5	63.4	84.2
Marinheiro et al. [24]	22.1	79.7	94.3	25.6	66.9	86.5	28.7	59.0	83.7
Marinheiro et al. [24] × F *	21.3	84.1	94.4	**22.9**	**76.1**	**92.8**	25.4	66.5	87.2
Equation (7)	25.2	63.2	93.8	29.1	60.3	82.0	29.7	58.3	83.4
Equation (7) × F *	22.9	80.8	95.3	25.4	68.1	89.2	26.0	66.6	89.3

* These correlations, shaded in gray, have just one flow regime and have been corrected by angle factor, Equations (8), and (9). ** The blue shaded cells are correlations which account for the flow inclination angle. *** Moser et al. [16], with the Zhang and Webb [58] pressure drop model. The best-performed MAPE, λ_{30} and λ_{50} for each group is in bold and underlined.

Table 6. Comparison of predictive methods for the database in Table 2, subdivided by flow pattern according to the flow pattern map of El Hajal et al. [46] for horizontal flow.

Methods/Databases	Stratified (83 Points)			Stratified Wavy (3200 Points)			Intermittent (485 Points)			Annular (1091 Points)			Mist (85 Points)		
	MAPE [%]	$\lambda_{30\%}$ [%]	$\lambda_{50\%}$ [%]	MAPE [%]	$\lambda_{30\%}$ [%]	$\lambda_{50\%}$ [%]	MAPE [%]	$\lambda_{30\%}$ [%]	$\lambda_{50\%}$ [%]	MAPE [%]	$\lambda_{30\%}$ [%]	$\lambda_{50\%}$ [%]	MAPE [%]	$\lambda_{30\%}$ [%]	$\lambda_{50\%}$ [%]
Akers et al. [51]	71.1	41.0	50.6	59.3	44.5	62.6	74.9	21.4	33.8	47.2	35.1	59.2	49.5	1.2	55.3
Traviss et al. [52]	54.8	12.0	28.9	38.1	53.9	79.6	34.4	66.8	80.8	47.2	47.7	72.2	19.7	85.9	90.6
Cavallini and Zecchin [18]	56.2	15.7	30.1	31.3	59.6	84.3	31.6	65.8	85.8	35.3	59.8	90.7	16.6	85.9	95.3
Shah [19]	61.8	12.0	21.7	28.9	58.3	83.5	22.3	73.8	88.0	26.2	70.9	89.4	22.9	75.3	92.9
Shah [19] × F *	40.4	42.2	61.4	**24.3**	**70.9**	**89.8**	23.5	75.5	87.6	26.7	67.6	90.2	22.9	75.3	92.9
Moser et al. [16]	53.9	16.9	32.5	34.9	55.8	80.1	20.2	81.2	93.8	28.5	75.5	88.1	21.8	74.1	**100**
Chang et al. [53]	65.3	10.8	19.3	36.9	37.8	74.6	22.9	73.8	95.3	26.6	61.2	86.4	33.3	37.6	90.6
Moser et al. [16] modified ***	55.5	15.7	21.7	61.0	28.2	63.8	24.9	71.8	95.5	29.8	54.9	87.2	18.0	80.0	**100**
Bohdal et al. [54]	35.2	61.4	85.5	78.5	28.4	47.0	87.9	14.8	23.3	65.5	21.2	45.2	77.3	0	7.1
Kim and Mudawar [23]	46.3	28.9	47.0	35.2	48.6	80.7	26.9	69.9	90.7	31.6	64.0	84.4	38.9	21.2	82.4
Mohseni et al. [12] **	25.8	**79.5**	**88.0**	100.8	31.8	43.0	77.3	15.9	44.9	85.8	30.2	42.6	43.8	34.1	62.4
Yang et al. [25] **	48.8	37.3	61.4	52.0	23.5	44.4	61.4	7.8	26.0	53.5	18.4	38.6	74.9	0	0
Xing et al. [26] **	1266.8	14.5	22.9	33.6	57.6	79.8	18.2	80.2	95.3	24.5	73.5	92.2	15.1	**88.2**	**100**
Macdonald and Garimella [55]	47.9	31.3	56.6	57.5	28.7	57.9	69.8	41.9	72.2	129.6	27.0	45.3	398.2	3.5	5.9
Cao et al. [28] **	81.4	49.4	65.1	35.2	55.7	79.7	20.2	78.1	91.8	29.6	62.6	83.2	15.8	**88.2**	**100**
Dorao and Fernandino [20]	70.0	3.6	18.1	39.1	35.6	67.2	18.1	83.7	98.6	**20.6**	77.4	91.7	20.9	72.9	**100**
Dorao and Fernandino [20] × F *	53.9	19.3	48.2	33.6	49.0	74.0	**16.0**	89.1	98.6	20.7	78.4	92.3	20.9	72.9	**100**
Dorao and Fernandino [21]	40.9	51.8	62.7	28.9	57.8	84.1	16.6	**91.1**	**99.0**	21.2	**79.0**	92.9	20.9	72.9	**100**
Murphy et al. [17]	61.9	2.4	25.3	58.1	35.7	61.5	79.4	35.7	40.0	92.3	31.3	41.0	84.6	12.9	24.7
Hosseini et al. [56]	54.8	50.6	60.2	32.6	50.8	86.1	22.6	62.1	92.6	24.4	66.5	91.8	19.9	77.6	95.3
Moghadam et al. [27] **	52.9	36.1	54.2	55.8	39.1	58.9	73.9	19.0	31.3	49.9	34.3	52.8	70.5	7.1	7.1
Shah [22] **	27.1	63.9	83.1	26.7	66.3	86.8	17.5	82.5	96.7	26.1	75.3	92.9	**15.0**	**88.2**	**100**
Nie et al. [57]	**25.0**	67.5	85.5	27.8	63.6	83.1	24.7	67.6	94.8	22.5	72.0	92.9	26.4	65.9	97.6
Marinheiro et al. [24]	51.6	16.9	51.8	28.9	59.2	82.0	18.5	84.9	96.5	21.7	77.0	96.2	39.4	21.2	81.2
Marinheiro et al. [24] × F *	33.8	57.8	69.9	25.2	69.3	87.4	17.2	88.5	96.5	21.9	77.2	96.5	39.4	21.2	81.2
Equation (7)	60.9	7.2	26.5	31.8	50.3	79.0	18.8	88.0	97.3	22.7	78.4	97.5	26.0	60.0	**100**
Equation (7) × F *	38.2	44.6	65.1	27.0	64.4	86.8	17.7	89.9	97.3	23.0	75.6	**97.7**	26.0	60.0	**100**

* These correlations, shaded in gray, have just one flow regime and have been corrected by angle factor, Equations (8), and (9). ** The blue shaded cells are correlations which account for the flow inclination angle. *** Moser et al. [16], with the Zhang and Webb [58] pressure drop model. The best-performed MAPE, λ_{30} and λ_{50} for each group is in bold and underlined.

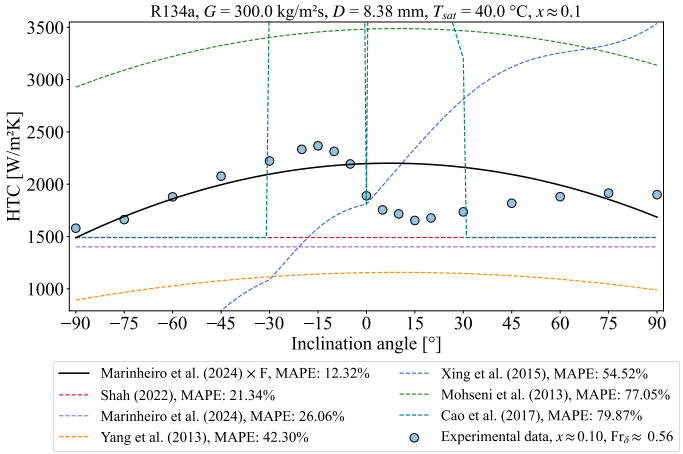
Table 7 shows the MAPE for correlations that explicitly account for the inclination angle in their original formulations, Xing et al. [26], Cao et al. [28], Shah [22], Yang et al. [5], compared to the Marinheiro et al. [24] × F correlation for each angle covered by the database. The most accurate correlations exhibit similar MAPE values for all inclinations angles included in the database.

Table 7. MAPE for the Xing et al. [26], Cao et al. [28], Shah [22], Yang et al. [5], and Marinheiro et al. [24] × F correlations for each angle of the database. Angles were grouped in 15-degree increments.

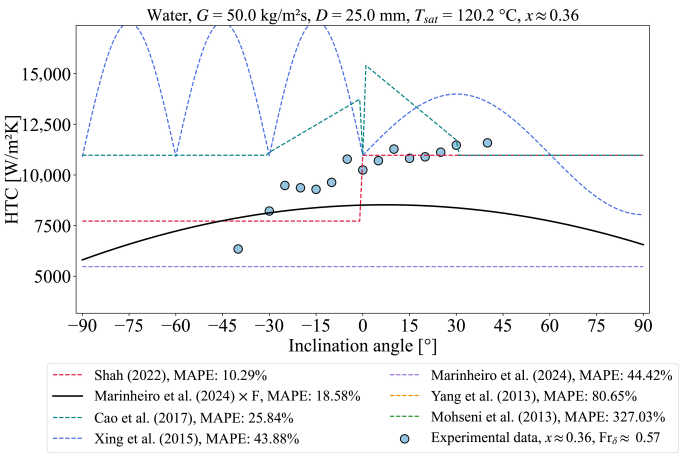
Angle [°]	Yang et al. [25]	Xing et al. [26]	Cao et al. [28]	Shah [22]	Marinheiro et al. [24] × F
−90	65.23	85.89	24.85	**24.80**	32.49
−75	38.52	118.08	21.65	21.65	**20.48**
−60	46.75	34.69	20.06	20.02	**16.13**
−45	52.93	40.24	23.29	23.29	**22.90**
−30	40.85	36.91	40.84	27.05	**17.86**
−15	48.75	53.99	49.25	21.75	**12.87**
0	51.29	21.62	21.64	**17.16**	21.38
15	32.03	**20.95**	96.69	22.77	23.16
30	34.93	31.51	41.46	27.08	**22.07**
45	39.73	29.76	26.15	26.15	**11.90**
60	50.73	38.39	33.15	33.15	**27.23**
75	34.26	18.17	16.81	16.81	**7.88**
90	58.94	46.96	28.32	36.76	**22.04**

The MAPE of the correlation with the best performance for each group is in bold and underlined.

Figure 11 presents the parametric effect of the inclination angle on the HTC for some correlations that exhibited the lowest MAPEs. The experimental data shown correspond to $Fr_\delta < 1$, conditions characterized by relevant influence of flow orientation, as established by the criterion defined in Equation (6). The first remark is that only a few correlations capture the parametric effect of the inclination angle on the HTC, which can generally be summarized as higher HTCs for near-horizontal inclinations and higher HTCs for upward flow compared to downward orientations. The proposed correction factor F seems to replicate this behavior and, in some cases, it captures the experimental trends with reasonable accuracy, as shown in Figure 11a,c,d,f.



(**a**)



(**b**)

Figure 11. *Cont.*

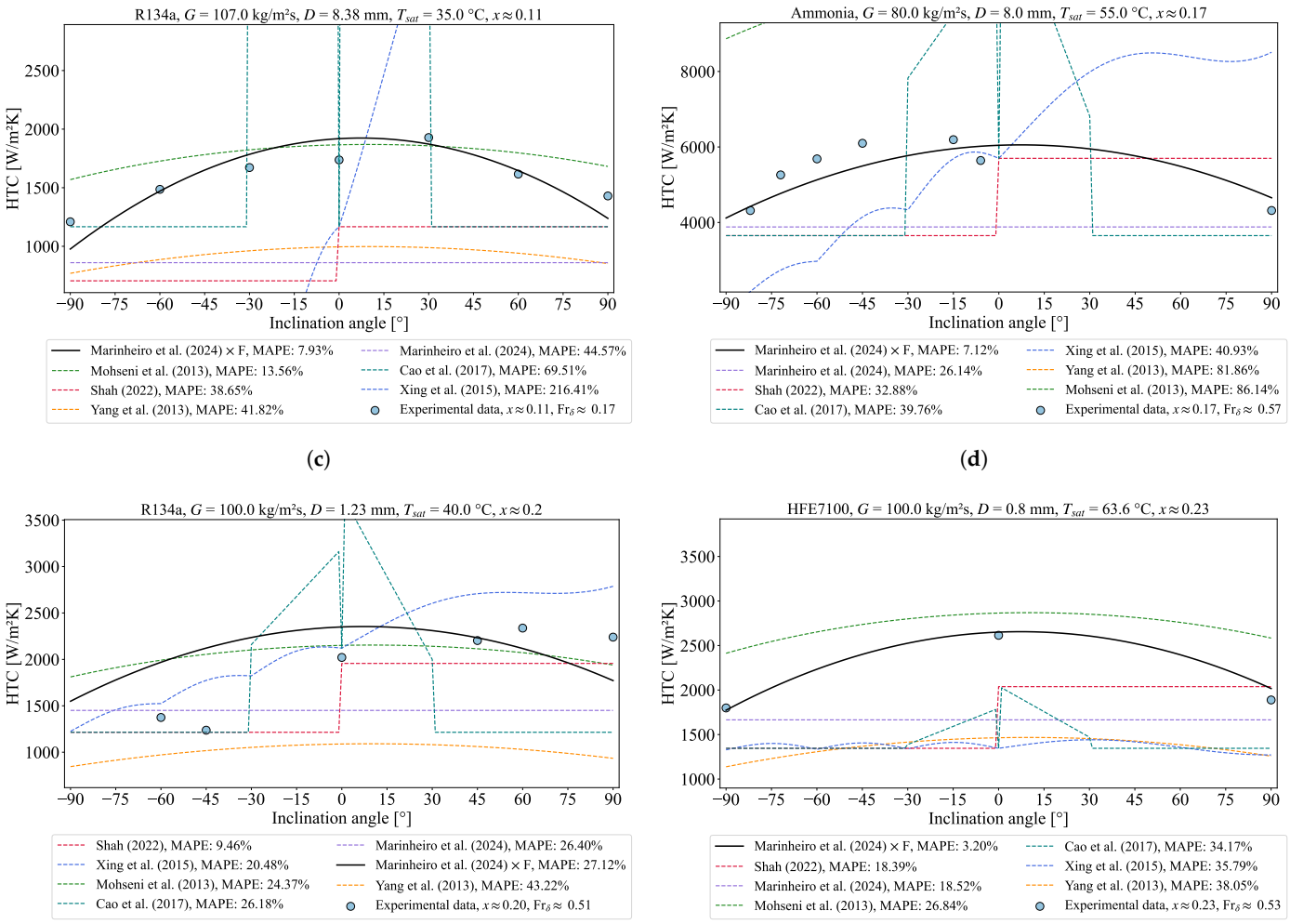


Figure 11. Parametric comparison of predicted HTC as a function of the tube inclination for different experimental data and predictive methods with inclination factor. Cao et al. (2017) corresponds to [28]; Marinheiro et al. (2024) corresponds to [24]; Mohseni et al. (2013) corresponds to [12]; Shah (2022) corresponds to [22]; Xing et al. (2015) corresponds to [26]; and Yang et al. (2013) corresponds to [25]. (**a**) Data from Lips and Meyer [8]. (**b**) Data from Yang et al. [5]. (**c**) Data from Mohseni et al. [12]. (**d**) Data from Ruzaikin et al. [43]. (**e**) Data from Del Col et al. [13,38]. (**f**) Data from Lin and Wang [42].

Figure 12 compares the parametric effect of inclination angle for the correlations originally proposed by Shah [19], Dorao and Fernandino [20] and Marinheiro et al. [24], and their corresponding corrections incorporating factor F, seen in Equation (8). The comparison was also performed by the correlation adjusted in the present study, outlined in Equation (7). The selected experimental data are similar to those shown in Figure 11. Although the parametric effect is similar for all correlations, the absolute values of HTC can vary considerably, with differences exceeding 30%. Therefore, special attention is recommended when selecting a correlation, ensuring that its range of applicability is respected, particularly given the current diversity of fluids used in applications.

Figure 13 compares the experimental HTC and the corresponding predictions according to Shah [19] and Marinheiro et al. [24], corrected by factor F, seen in Equation (8), for data points with Fr_δ values above and below the threshold of 4.75. It is clear that for Fr_δ above 4.75, the inclination effect is reduced for both experimental and predicted HTCs, reinforcing the notion that the influence of gravitational forces is diminished at $Fr_\delta > 4.75$.

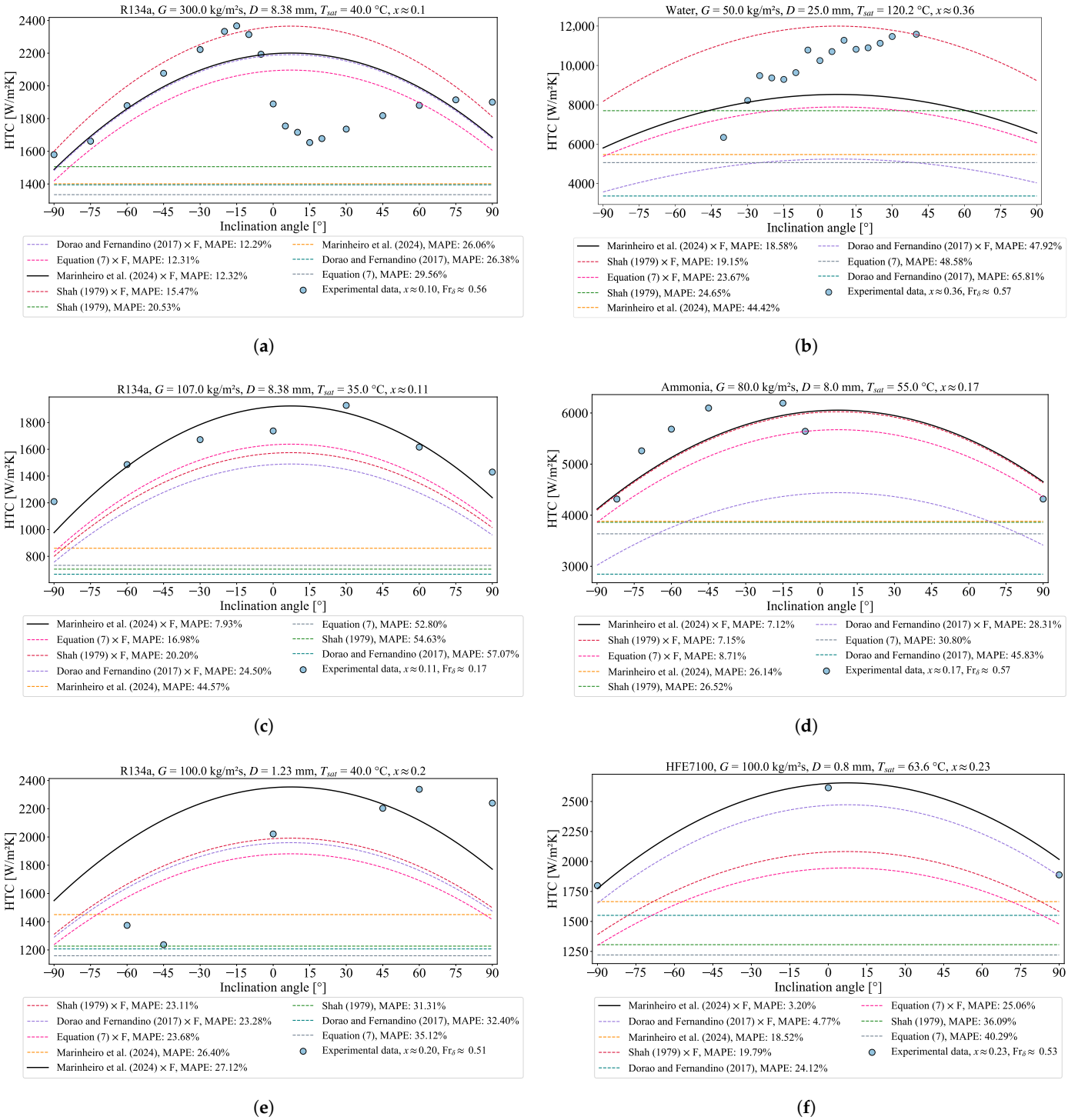
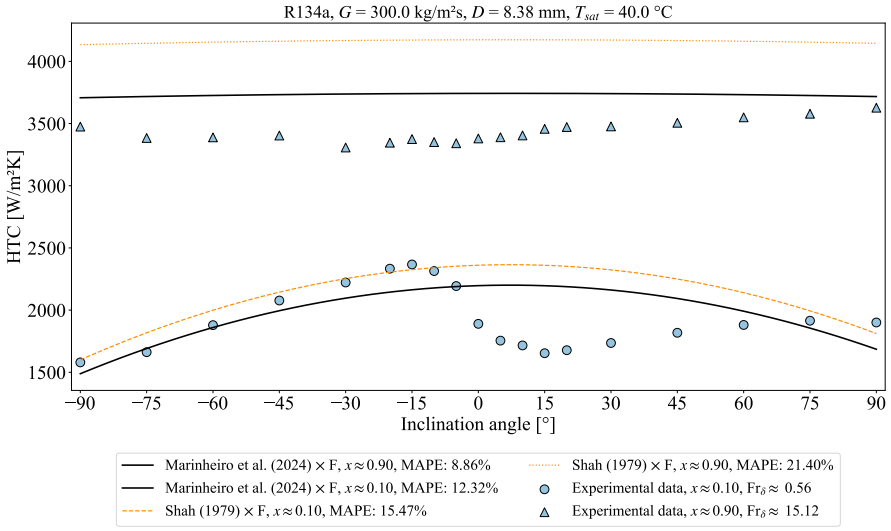


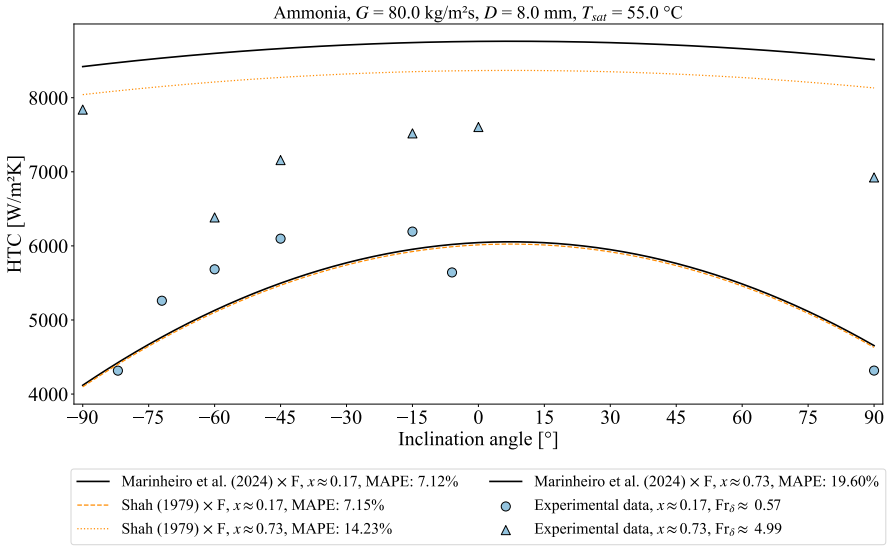
Figure 12. Parametric comparison of predicted HTC as a function of the tube inclination for different experimental data and predictive methods without inclination factor and corrected by F. Dorao and Fernandino corresponds to [20]; Marinheiro et al. (2024) corresponds to [24]; and Shah (1979) corresponds to [19]. (**a**) Data from Lips and Meyer [8]. (**b**) Data from Yang et al. [5]. (**c**) Data from Mohseni et al. [12]. (**d**) Data from Ruzaikin et al. [43]. (**e**) Data from Del Col et al. [13,38]. (**f**) Data from Lin and Wang [42].

As a final analysis, microgravity condensation data from Mudawar et al. [59] is compared with Equation (7) correlation to verify the hypothesis that, for $Fr_\delta > 4.75$, gravity forces have minimal influence on heat transfer under Earth gravity conditions. If this hypothesis is valid, Equation (7) should provide small deviations for microgravity data, since, as discussed in Section 4, this correlation was adjusted only using experimental data

for $Fr_\delta > 4.75$. Table 8 presents the statistical results of the comparisons against 1093 local HTC data under microgravity, collected from Mudawar et al. [59] for n-Perfluorohexane condensation in a 7.24 mm diameter channel, at mass velocities of 72.8–291.5 kg/m^{2}s and local vapor qualities ranging from 0 to 1. The Fr_δ values for these data vary from $2.1 \cdot 10^{-5}$ to 10.3. Based on the criteria established by Equation (6), if these data had been obtained under normal gravity, about 82% of the tested conditions (data with $Fr_\delta < 4.75$) would be affected by gravity force.



(**a**)

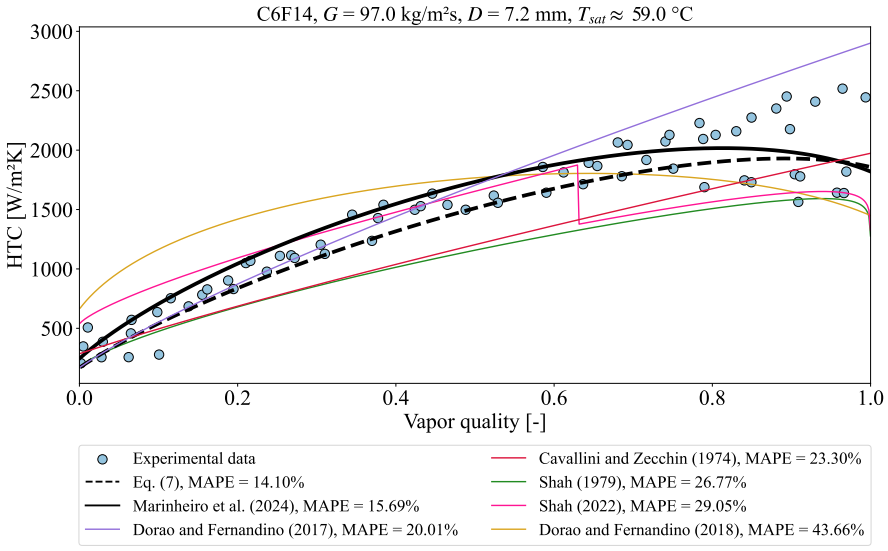


(**b**)

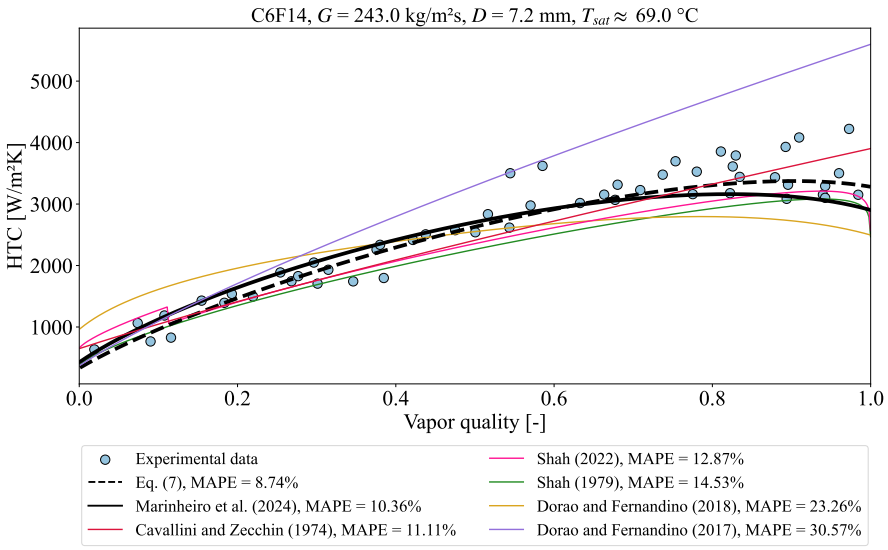
Figure 13. Parametric comparison of predicted HTC for Shah [19] and Marinheiro et al. [24] correlations corrected by F as a function of the tube inclination for different experimental data. Marinheiro et al. (2024) corresponds to [24]; Shah (1979) corresponds to [19]. (**a**) Data from Lips and Meyer [8]; (**b**) data from Ruzaikin et al. [43].

According to Table 8, Equation (7) predicted the microgravity data with the lowest MAPE, 19.5%, which is smaller than the mean absolute percentage error obtained by the same correlation when compared to data under normal gravity conditions (Table 3). The correlation of Marinheiro et al. [24] also showed a reasonable performance, as expected, since it shares the same functional form as Equation (7) and its regression database contains nearly 70% of data with $Fr_\delta > 4.75$. It should be noted that, for the comparison against

microgravity experimental data, the gravitational acceleration used in all correlations and their corresponding criteria was kept at the terrestrial value of 9.81 m/s^2. For correlations that depend on the inclination angle, the horizontal flow orientation (θ = 0°) was assumed. The correction factor F, was not applied in the comparisons summarized in Table 8, as it has no significance under microgravity conditions. Care should be taken when altering the gravitational acceleration constant in correlations, since most of them were developed using terrestrial g = 9.81 m/s^2 as a fixed value. Figure 14 shows a parametric trend comparison of some correlations against microgravity data. It can be noted that the HTC against vapor quality trends are accurately captured by the best performance correlations. This analysis reveals that microgravity data can be accurately predicted by correlations developed under normal terrestrial gravity conditions, such as those proposed in the present study, Equation (7), and by Marinheiro et al. [24], which account for the key effects of gravitational forces on inertia and viscous phenomena.



(**a**)



(**b**)

Figure 14. Parametric comparison of predicted HTC for Cavallini and Zecchin [18], Shah [19], Dorao and Fernandino [20], Dorao and Fernandino [21], Shah [22], and Marinheiro et al. [24] correlations and (7) as a function of the local vapor quality for the microgravity data from Mudawar et al. [59]. (**a**) Data for G = 97 kg/m^{2}s and T_{sat} = 59 °C; (**b**) data for G = 243 kg/m^{2}s and T_{sat} = 69 °C.

Table 8. Comparison of predictive methods for microgravity experimental data of Mudawar et al. [59].

Methods/Databases	Mudawar et al. [59] Database (1093 Points)		
	MAPE [%]	$\lambda_{30\%}$ [%]	$\lambda_{50\%}$ [%]
Akers et al. [51]	36.1	67.8	83.1
Traviss et al. [52]	26.7	76.6	88.7
Cavallini and Zecchin [18]	23.0	80.5	94.7
Shah [19]	27.3	68.2	93.9
Moser et al. [16]	31.2	56.9	93.6
Chang et al. [53]	39.0	21.0	91.9
Moser et al. [16] modified **	32.9	54.0	93.5
Bohdal et al. [54]	41.5	26.7	64.1
Kim and Mudawar [23]	26.6	69.4	94.6
Mohseni et al. [12] *	132.9	1.6	1.9
Yang et al. [25] *	40.8	58.4	76.6
Xing et al. [26] *	23.1	84.1	92.4
Macdonald and Garimella [55]	25.6	73.9	**95.2**
Cao et al. [28] *	23.1	84.1	92.4
Dorao and Fernandino [20]	31.0	58.6	91.7
Dorao and Fernandino [21]	33.3	68.3	86.9
Murphy et al. [17]	28.7	67.2	88.8
Hosseini et al. [56]	49.1	54.9	70.8
Moghadam et al. [27] *	35.3	47.2	83.5
Shah [22] *	23.1	84.2	92.5
Nie et al. [57]	21.0	83.7	91.3
Marinheiro et al. [24]	19.9	86.7	94.7
Equation (7)	**19.5**	**87.8**	93.0

* The blue shaded cells are correlations which account for the flow inclination angle and, in this case, $\theta = 0°$ was considered. ** Moser et al. [16] with the Zhang and Webb [58] pressure drop model. The best-performed MAPE, λ_{30} and λ_{50} for each group is in bold and underlined.

6. Conclusions

This work analyzed the effect of flow inclination on the heat transfer coefficient for internal flow condensation. An extensive literature review was performed, experimental data was compared against state-of-the-art correlations, and new prediction methods were proposed. The main findings are listed below:

- A criterion to distinguish flow regime conditions in which the inclination angle is significant was developed, as given by Equation (6). It was found that for a liquid film thickness Froude number $Fr_\delta < 4.75$, the inclination angle plays a relevant role in internal flow condensation.
- A correction factor, F, was proposed to predict the HTC in inclined channels, shown in Equations (8) and (9). The correction factor is a function of both the inclination angle and the liquid film thickness Froude number. It indicates that asymmetry in the liquid film thickness increases the average circumferential heat transfer coefficient (HTC), with a more pronounced effect for upward flows. This finding suggests that buoyancy forces positively contribute to heat transfer in upward flow conditions.
- Comparisons between prediction methods, coupled to the newly developed inclination correction factor, and experimental data revealed a consistent reduction in deviations due to the incorporation of Equations (8) and (9). Among all tested prediction methods, the lowest mean absolute percentage error, 24.1%, for the inclined tube database was obtained by the correlation of Marinheiro et al. [24] multiplied by the inclination correction factor proposed. This represents an improvement from the 26.9% error obtained with the same correlation without the inclination correction. Comparable MAPE reduction from 28.1% to 25.0% was achieved by the correlation of Shah [19].

- Comparisons between microgravity HTC data of Mudawar et al. [59] and the evaluated correlations show that Equation (7), developed for $Fr_\delta > 4.75$, predicted the microgravity database with the lowest MAPE. This result supports the assumption that, under normal Earth gravity conditions, gravitational forces are less relevant for condensing flows with $Fr_\delta > 4.75$.

Author Contributions: Data analysis, methods, and writing: M.H.C., V.G.F., A.G.C., M.M.D., M.M.M., D.B.M., and C.B.T. Supervision and text integration: C.B.T. All authors have read and agreed to the published version of the manuscript.

Funding: This research was funded by FAPESP (The State of São Paulo Research Foundation, Brazil), Contract 2019/22105-5, 2019/11066-9, 2022/15765-1, 2022/02665-9, 2024/20072-0, by the Coordination of Superior Level Staff Improvement–Brazil (CAPES)—Financing Code 001, National Council for Scientific and Technological Development (CNPq), Grant No. 310179/2021-1, 305865/2024-2, 141440/2024-4 and Petrobras/FIPAI 010/24.

Data Availability Statement: The dataset is available on request from the authors.

Acknowledgments: The authors acknowledge the financial support given by FAPESP (The State of São Paulo Research Foundation, Brazil) Contract 2019/11066-9, 2022/15765-1, 2022/02665-9, by Coordination of Superior Level Staff Improvement–Brazil (CAPES)–Financing Code 001, National Council for Scientific and Technological Development (CNPq), Grant No. 310179/2021-1, 305865/2024-2, 141440/2024-4 and Petrobras/FIPAI 010/24.

Conflicts of Interest: The authors declare that this study received funding from company Petrobras. The funder was not involved in the study design, collection, analysis, interpretation of data, the writing of this article or the decision to submit it for publication.

Abbreviations

The following abbreviations are used in this manuscript:

CFC	Chlorofluorocarbon
D	Downward
H	Horizontal
HFC	Hydrofluorocarbon
HFE	Hydrofluoroethers
HFO	Hydrofluoroolefin
HTC	Heat transfer coefficient
MAPE	Mean absolute percentage error
U	Upward

Symbols

The following symbols are used in this manuscript:

Bd	Bond number [-], $D\sqrt{\frac{g(\rho_l-\rho_v)}{\sigma}}$
D	Diameter [mm]
F	Correction factor [-]
Fr	Froude number [-], $\frac{G^2}{gD\rho^2}$
Fr_l	Liquid Froude number [-], $\frac{G^2(1-x)^2}{gD\rho_l^2}$
Fr_{lo}	Liquid-only Froude number [-], $\frac{G^2}{gD\rho_l^2}$
Fr_v	Vapor Froude number [-], $\frac{G^2x^2}{gD\rho_v^2}$
Fr_{vo}	Vapor-only Froude number [-], $\frac{G^2}{gD\rho_v^2}$
Fr_δ	Liquid film thickness Froude number [-]
G	mass velocity [kg/m^2]
g	Gravity [9.81 m/s^2]

h	Heat transfer coefficient [W/m^{2}K]
k	Thermal conductivity [W/mK]
L	Length [m]
Nu	Nusselt number [-], $\frac{hD}{k}$
p	Pressure [Pa]
Pr	Prandtl number [-], $\frac{\mu c_p}{k}$
Pr_{2p}	Two-phase Prandtl number [-], $\frac{\mu_l c_{p,l}(1-x)}{k_l} + \frac{\mu_v c_{p,v} x}{k_v}$
Re	Reynolds number [-], $\frac{GD}{\mu}$
Re_l	Liquid Reynolds number [-], $\frac{GD(1-x)}{\mu_l}$
Re_{lo}	Liquid-only Reynolds number [-], $\frac{GD}{\mu_l}$
Re_v	Vapor Reynolds number [-], $\frac{GDx}{\mu_v}$
Re_{vo}	Vapor-only Reynolds number [-], $\frac{GD}{\mu_v}$
Re_{2p}	Two-phase Reynolds number [-], $\frac{GD(1-x)}{\mu_l} + \frac{GDx}{\mu_v}$
T	Temperature [°C]
x	Vapor quality [-]
	Greek symbols
χ	Lockhart–Martinelli parameter [-]
χ_{tt}	Turbulent liquid and vapor phases Lockhart–Martinelli parameter [-], $\left(\frac{1-x}{x}\right)^{0.9}\left(\frac{\rho_v}{\rho_l}\right)^{0.5}\left(\frac{\mu_l}{\mu_v}\right)^{0.1}$
δ	Liquid film thickness [m]
λ_i	Percentage of data within the range of i% [%]
μ	Dynamic viscosity [Ns/m^2]
ρ	Density [kg/m^3]
θ	Inclination angles [°]
	Subscripts
$2p$	Two phase
b	Bottom
H	Hydraulic
l	Liquid
lo	Liquid-only
m	Average
r	Reduced
sat	Saturation
t	Top
v	Vapor
vo	Vapor-only
w	Tube wall

Appendix A. Selected Correlations for Analysis

Table A1. Summary of the experimental conditions considered for developing predictive methods for condensing HTC.

Author	Valid for Vertical or Inclined Tubes?/ Validity Range	Fluids	D_h[mm]	G [kg/m^{2}s]	T [°C]/p_r [-]	Other Remarks
HEAT–MOMENTUM ANALOGY						
Traviss et al. [52]	No/-	R12; R22	8.0	161.4–1532	24–60/-	Valid for horizontal flow Annular flow
Moser et al. [16]	Yes/−90°	R11; R113; R12; R125; R22; R134a; R410A	3.14–20	87–1532	21–79/0.017–0.651	Valid for horizontal and vertical downflow 1197 data points
Murphy et al. [17]	Yes/−90°	R290	1.93	75–150	47–74/0.38–0.66	Valid only for vertical downward flow Developed based on 27 data points
EMPIRICAL						
Akers et al. [51]	No/-	R12; R290	15.7	78–418	-/0.657–0.662	Valid for horizontal flow 32 data points
Cavallini and Zecchin [18]	No/-	R12; R22; R113	-	-	-	Valid for horizontal flow Annular flow $7000 \leq Re_LO \leq 53{,}000$
Shah [19]	Yes/−90° and −15°	Water; R11; R12; R22; R113; methanol; ethanol; benzene; toluene; trichloroethylene	7–40	10.8–210	21–310/0.002–0.44	Valid for horizontal, vertical down, and inclined flow 474 data points $0.158 < q'' < 1893$ kW/m^2 $1 < Pr_L < 13$
Chang et al. [53]	No/-	R290; R600; R600a; R1270; R290/R600; R290/R600a	8.0	50–350	-	Valid for horizontal flow Developed for pure fluids and binary mixtures of hydrocarbons, circular channel
Bohdal et al. [54]	No/-	R134a; R404A	0.31–3.30	100–1300	20–40/-	Valid for horizontal flow Single-channels, circular geometry

Table A1. *Cont.*

Author	Valid for Vertical or Inclined Tubes?/ Validity Range	Fluids	D_h[mm]	G [kg/m^{2}s]	T [°C]/p_r [-]	Other Remarks
Mohseni et al. [12]	Yes/−90°, −60°, −30°, 0°, +30°, +60° and +90°	R134a	8.38	53–212	35/ -	Valid for horizontal, vertical and inclined flow Single smooth tube
Yang et al. [25]	Yes/−30°	Water	50.0	10.33–14.15	85–103/-	Valid for inclined downflow $5000 \leq Re \leq 45{,}000$
Xing et al. [26]	Yes/−90°, −60°, −45°, −30°, −8°, −4°, 0°, +4°, +8°, +30°, +45°, +60° and +90°	R245fa	14.81	191.3–705.4	-/0.11–0.1117	Valid for horizontal, vertical and inclined flow Non-dimensional analysis combined with Shah [31] correlation
Cao et al. [28]	Yes/−30°, −15°, −10°, −5°, 0°, +5°, +10°, +15° and +30°	R245fa	14.7	198.8–504.7	63.1/0.1382	Shell-tube heat exchanger $0.291 \leq x \leq 0.946$
Dorao and Fernandino [20]	Yes/−90° and +90°	R125; R141b; R22; R236ea; R245fa; R134a; R410A; R32; R1234ze; R152a; R744; R32/R1234ze; R125/R236ea; R32/R125; water; and other 5 fluids not explicited	0.067–14.45	200–1360	−132–115/-	Valid for horizontal, vertical up and downflow 2784 data points Circular, Rectangular, Barrel, Triangular, W- shaped, N-shaped and circular channels
Dorao and Fernandino [21]	Yes/−90° and +90°	Water; R22; R407c; R410a; R134a; R410A; R32; R236ea; R125; R245fa; R32/R125; carbon dioxide; R1234ze; R141b; R152a; and other 5 fluids not explicited	0.067–20	45.5–1360	−132.3–115/-	Valid for horizontal, vertical up and downflow 3937 data points Circular, rectangular, barrel, triangular, W- shaped, N-shaped and semi-circular channels
Hosseini et al. [56]	No/-	R290, R170, R50, R728, R601, R600a, R290/R600a, R1270, R1234yf, R1234ze(E), R125, R134a, R14, R152a, R161, R22, R236ea, R245fa, R32, R32/R125, R404A, R407C, R41, R410A, R718	0.133–20.8	13.1–1200	0.0005–0.952	Valid for horizontal flow Circular and rectangular single channels 5809 data points

Table A1. *Cont.*

Author	Valid for Vertical or Inclined Tubes?/ Validity Range	Fluids	D_h[mm]	G [kg/m^{2}s]	T [°C]/p_r [-]	Other Remarks
Moghadam et al. [27]	Yes/−90°, −60°, −30°, 0°, +30°, +60° and +90°	R1234yf	8.3	80–320	25/0.2018	Valid for horizontal, vertical and inclined flow $1000 \leq Re_L \leq 14{,}000$ $2.8 \leq Pr_L \leq 3.2$
Shah [22]	Yes/−90°	Water, R11, R12, R22, R32, R41, R113, R123, R125, R134a, R141b, R142b, R152a, R161, R236ea, R245fa, R404A, R410A, R448A, R449A, R450A, R502, R507, R513A, R452B, R454C, R455A, R1234fa, R1234yf, R1234ze(E), DME, butane, propane, carbon dioxide, methane, FC-72, isobutane, propylene, benzene, ethanol, methanol, toluene, Dowtherm 209, HFE7000, HFE7100, ethane, pentane, Novec649, ammonia, nitrogen	0.08–49	1.1–1400	-/0.0006–0.949	Valid for horizontal and vertical downflow 8298 data points from 130 sources Circular, rectangular, semi-circular, annular, triangular and barrel-shaped single and multichannels
Nie et al. [57]	No/-	Ammonia, R744, DME, ethane, HFE-7000, methane, nitrogen, Novec649, R12, R123, R1234yf, R1234ze(E), R125, R1270, R134a, R14, R141b, R142b, R152a, R161, R22, R236ea, R245fa, R290, R32, R41, R600a, R601	0.49–8.92	13–1200	-/0.03–0.95	Valid for horizontal flow Circular single-channels 6064 data points from 49 sources
Marinheiro et al. [24]	Yes/−90°	Ammonia, Dimethylether, Ethane (R170), Ethane/R290(0.33/0.67), Ethane/R290(0.67/0.33), HFE7000, HFE7100, Methane (R50), Methane/Ethane(0.590/0.409), Methane/Ethane(0.828/0.172), Methane/Nitrogen(0.837/0.162), Nitrogen, Novec649, n-pentane (R601), Propylene (R1270), R12, R123, R1234yf, R1234ze(E), R125, R134a, R14, R141b, R142b, R152a, R161, R22, R236ea, R236fa, R245fa, R245fa/n pentane(0.088/0.912), R245fa/n pentane(0.45/0.55), R290, R32, R32/R1234ze(E)(0.23/0.77), R32/R1234ze(E)(0.25/0.75), R32/R1234ze(E)(0.45/0.55), R32/R1234ze(E)(0.46/0.54), R32/R1234ze(E)(0.748/0.251), R32/R1234ze(E)(0.75/0.25), R32/R125(0.5/0.5), R32/R134a(0.265/0.735), R32/R134a(0.55/0.45), R32/R134a(0.745/0.255), R404A, R407C, R41, R410A, R448A, R450A, R452A, R452B, R454B, R454C, R502, R507A, R513A, R600, R600a, R600a/Propylene(0.8056/0.1944), R600a/R290(0.5/0.5), R600a/R290(0.7546 /0.2454), R744, R744/Dimethylether(0.21/0.79), R744 /Dimethylether(0.39/0.61), R744/Nitrogen(0.967/0.033), R744/Nitrogen(0.980/0.02), R744/Nitrogen(0.994/0.006), Water.	0.0667–20.8	13.1–1400	-/0.0313– 0.998	Valid for horizontal and vertical downflow 69 working fluids, 12,017 data points Circular, rectangular, triangular, semi-circular and flattened channels

Table A1. *Cont.*

Author	Valid for Vertical or Inclined Tubes?/ Validity Range	Fluids	D_h[mm]	G [kg/m^{2}s]	T [°C]/p_r [-]	Other Remarks
FLOW-PATTERN-BASED						
Conventional channels						
Macdonald and Garimella [55]	No/-	Propane; pentane	7.75–14.45	150–600	30–94/0.04–0.95	Valid for horizontal flow Single channels
Minichannels						
Kim and Mudawar [23]	Yes/−90° and +90°	R12; R22; R134a; R404A; R123; CO2; R410A; methane; R600a; R32; R245fa; R1234yf; R236fa; R1234ze(E); FC72	0.424–6.22	53–1403	-/0.04–0.91	Valid for horizontal, vertical up and downflow First correlation to include vertical upward data points 4045 data points Circular and rectangular single and multichannels $276 \leq Re_{LO} \leq 89{,}798$

References

1. Ahn, T.; Kang, J.; Bae, B.; Jeong, J.J.; Yun, B. Steam condensation in horizontal and inclined tubes under stratified flow conditions. *Int. J. Heat Mass Transf.* **2019**, *141*, 71–87. [CrossRef]
2. Goto, T.; Jige, D.; Inoue, N.; Sagawa, K. Condensation flow visualization, heat transfer, and pressure drop in printed circuit heat exchangers with straight and wavy microchannels. *Int. J. Refrig.* **2023**, *152*, 234–240. [CrossRef]
3. Lips, S.; Meyer, J.P. Two-phase flow in inclined tubes with specific reference to condensation: A review. *Int. J. Multiph. Flow* **2011**, *37*, 845–859. [CrossRef]
4. Adelaja, A.O.; Dirker, J.; Meyer, J.P. Experimental study of the pressure drop during condensation in an inclined smooth tube at different saturation temperatures. *Int. J. Heat Mass Transf.* **2017**, *105*, 237–251. [CrossRef]
5. Yang, P.; Cao, X.; Liu, J.; Zhou, S. Experimental study of steam condensation heat transfer in an inclined tube at low mass fluxes. *Int. J. Heat Mass Transf.* **2024**, *224*, 125257. [CrossRef]
6. Kharangate, C.R.; Lee, H.; Park, I.; Mudawar, I. Experimental and computational investigation of vertical upflow condensation in a circular tube. *Int. J. Heat Mass Transf.* **2016**, *95*, 249–263. [CrossRef]
7. Ong, C.L.; Thome, J. Macro-to-microchannel transition in two-phase flow: Part 1–Two-phase flow patterns and film thickness measurements. *Exp. Therm. Fluid Sci.* **2011**, *35*, 37–47. [CrossRef]
8. Lips, S.; Meyer, J.P. Experimental study of convective condensation in an inclined smooth tube. Part I: Inclination effect on flow pattern and heat transfer coefficient. *Int. J. Heat Mass Transf.* **2012**, *55*, 395–404. [CrossRef]
9. Chato, J.C. Laminar Condensation Inside horizontal and Inclined Tubes. Ph.D. Thesis, Massachusetts Institute of Technology, Cambridge, MA, USA, 1960.
10. Meyer, J.P.; Dirker, J.; Adelaja, A.O. Condensation heat transfer in smooth inclined tubes for R134a at different saturation temperatures. *Int. J. Heat Mass Transf.* **2014**, *70*, 515–525. [CrossRef]
11. Ewim, D.R.E.; Meyer, J.P.; Abadi, S.N.R. Condensation heat transfer coefficients in an inclined smooth tube at low mass fluxes. *Int. J. Heat Mass Transf.* **2018**, *123*, 455–467. [CrossRef]
12. Mohseni, S.; Akhavan-Behabadi, M.; Saeedinia, M. Flow pattern visualization and heat transfer characteristics of R-134a during condensation inside a smooth tube with different tube inclinations. *Int. J. Heat Mass Transf.* **2013**, *60*, 598–602. [CrossRef]
13. Del Col, D.; Bortolato, M.; Azzolin, M.; Bortolin, S. Effect of inclination during condensation inside a square cross section minichannel. *Int. J. Heat Mass Transf.* **2014**, *78*, 760–777. [CrossRef]
14. Azzolin, M.; Bortolin, S.; Del Col, D. Convective condensation at low mass flux: Effect of turbulence and tube orientation on the heat transfer. *Int. J. Heat Mass Transf.* **2019**, *144*, 118646. [CrossRef]
15. Marchetto, D.B.; Marinheiro, M.M.; de Souza Netto, A.T.; Furlan, G.; Ribatski, G.; Thome, J.R.; Tibirica, C.B. Condensation flow inside tubes: A review of heat transfer coefficient measurement techniques, experimental databases and prediction methods. *Exp. Therm. Fluid Sci.* **2025**, *160*, 111298. [CrossRef]
16. Moser, K.W.; Webb, R.L.; Na, B. A New Equivalent Reynolds Number Model for Condensation in Smooth Tubes. *J. Heat Transf.* **1998**, *120*, 410–417. [CrossRef]
17. Murphy, D.L.; Macdonald, M.P.; Mahvi, A.J.; Garimella, S. Condensation of propane in vertical minichannels. *Int. J. Heat Mass Transf.* **2019**, *137*, 1154–1166. [CrossRef]
18. Cavallini, A.; Zecchin, R. A dimensionless correlation for heat transfer in forced convection condensation. In Proceedings of the International Heat Transfer Conference, Tokyo, Japan, 3–7 September 1974; Digital Library; Begel House Inc.: Danbury, CT, USA, 1974, pp. 309–313.
19. Shah, M. A general correlation for heat transfer during film condensation inside pipes. *Int. J. Heat Mass Transf.* **1979**, *22*, 547–556. [CrossRef]
20. Dorao, C.A.; Fernandino, M. Dominant dimensionless groups controlling heat transfer coefficient during flow condensation inside pipes. *Int. J. Heat Mass Transf.* **2017**, *112*, 465–479. [CrossRef]
21. Dorao, C.A.; Fernandino, M. Simple and general correlation for heat transfer during flow condensation inside plain pipes. *Int. J. Heat Mass Transf.* **2018**, *122*, 290–305. [CrossRef]
22. Shah, M.M. Improved correlation for heat transfer during condensation in mini and macro channels. *Int. J. Heat Mass Transf.* **2022**, *194*, 123069. [CrossRef]
23. Kim, S.M.; Mudawar, I. Universal approach to predicting heat transfer coefficient for condensing mini/micro-channel flow. *Int. J. Heat Mass Transf.* **2013**, *56*, 238–250. [CrossRef]
24. Marinheiro, M.M.; Marchetto, D.B.; Furlan, G.; de Souza Netto, A.T.; Tibiriçá, C.B. A robust and simple correlation for internal flow condensation. *Appl. Therm. Eng.* **2024**, *236*, 121811. [CrossRef]
25. Yang, J.G.; Ju, X.L.; Ye, S. An empirical correlation for steam condensing and flowing downward in a 50mm diameter inclined tube. *Adv. Mater. Res.* **2013**, *732*, 67–73. [CrossRef]
26. Xing, F.; Xu, J.; Xie, J.; Liu, H.; Wang, Z.; Ma, X. Froude number dominates condensation heat transfer of R245fa in tubes: Effect of inclination angles. *Int. J. Multiph. Flow* **2015**, *71*, 98–115. [CrossRef]

27. Moghadam, M.T.; Behabadi, M.A.; Sajadi, B.; Razi, P.; Zakaria, M.I. Experimental study of heat transfer coefficient, pressure drop and flow pattern of R1234yf condensing flow in inclined plain tubes. *Int. J. Heat Mass Transf.* **2020**, *160*, 120199. [CrossRef]
28. Cao, S.; Xu, J.; Li, Y.; Yan, Y. Condensation heat transfer of R245fa in a shell-tube heat exchanger at slightly inclined angles. *Int. J. Therm. Sci.* **2017**, *115*, 197–209. [CrossRef]
29. Boyko, L.; Kruzhilin, G. Heat transfer and hydraulic resistance during condensation of steam in a horizontal tube and in a bundle of tubes. *Int. J. Heat Mass Transf.* **1967**, *10*, 361–373. [CrossRef]
30. Akhavan-Behabadi, M.; Kumar, R.; Mohseni, S. Condensation heat transfer of R-134a inside a microfin tube with different tube inclinations. *Int. J. Heat Mass Transf.* **2007**, *50*, 4864–4871. [CrossRef]
31. Shah, M.M. An improved and extended general correlation for heat transfer during condensation in plain tubes. *Hvac&R Res.* **2009**, *15*, 889–913.
32. Dobson, M.K.; Chato, J.C. Condensation in smooth horizontal tubes. *ASME J. Heat Transf.* **1998**, *120*, 193–213. [CrossRef]
33. Brown, W.; Goodykoontz, J. *Local Heat-Transfer and Pressure Distributions for Freon-113 Condensing in Downward Flow in a Vertical Tube*; Technical Report; National Aeronautics and Space Administration—NASA: Washington, DC, USA, 1967.
34. Goodykoontz, J.H.; Dorsch, R.G. *Local Heat-Transfer Coefficients and Static Pressures for Condensation of High-Velocity Steam Within a Tube*; Technical report; National Aeronautics and Space Administration—NASA: Washington, DC, USA, 1967.
35. Maråk, K.A. Condensation Heat Transfer and Pressure Drop for Methane and Binary Methane Fluids in Small Channels. Ph.D. Thesis, Norges Teknisk-Naturvitenskapelige Universitet, Trondheim, Norway, 2009.
36. Dalkilic, A.; Laohalertdecha, S.; Wongwises, S. Experimental investigation of heat transfer coefficient of R134a during condensation in vertical downward flow at high mass flux in a smooth tube. *Int. Commun. Heat Mass Transf.* **2009**, *36*, 1036–1043. [CrossRef]
37. Park, J.E.; Vakili-Farahani, F.; Consolini, L.; Thome, J.R. Experimental study on condensation heat transfer in vertical minichannels for new refrigerant R1234ze (E) versus R134a and R236fa. *Exp. Therm. Fluid Sci.* **2011**, *35*, 442–454. [CrossRef]
38. Del Col, D.; Bortolato, M.; Bortolin, S.; Azzolin, M. Minichannel condensation in downward, upward and horizontal configuration. *J. Phys. Conf. Ser.* **2012**, *395*, 012092. [CrossRef]
39. Lips, S.; Meyer, J.P. Stratified flow model for convective condensation in an inclined tube. *Int. J. Heat Fluid Flow* **2012**, *36*, 83–91. [CrossRef]
40. Xie, J.; Xu, J.; Cheng, Y.; Xing, F.; He, X. Condensation heat transfer of R245fa in tubes with and without lyophilic porous-membrane-tube insert. *Int. J. Heat Mass Transf.* **2015**, *88*, 261–275. [CrossRef]
41. Olivier, S.P.; Meyer, J.P.; De Paepe, M.; De Kerpel, K. The influence of inclination angle on void fraction and heat transfer during condensation inside a smooth tube. *Int. J. Multiph. Flow* **2016**, *80*, 1–14. [CrossRef]
42. Lin, K.W.; Wang, C.C. Enhanced condensation heat transfer for dielectric fluid within microchannel heat sink. *Int. J. Heat Mass Transf.* **2017**, *106*, 518–525. [CrossRef]
43. Ruzaikin, V.; Lukashov, I.; Breus, A. Ammonia condensation in the horizontal and vertical smooth tubes. *Int. J. Refrig.* **2024**, *164*, 1–11. [CrossRef]
44. O'Neill, L.E.; Balasubramaniam, R.; Nahra, H.K.; Hasan, M.M.; Mudawar, I. Flow condensation heat transfer in a smooth tube at different orientations: Experimental results and predictive models. *Int. J. Heat Mass Transf.* **2019**, *140*, 533–563. [CrossRef]
45. Pusey, A.; Kwack, D.; Kim, H. Heat transfer coefficient and cross-sectional flow structure in condensation of steam in an inclined tube at a low mass flux. *Exp. Therm. Fluid Sci.* **2021**, *127*, 110414. [CrossRef]
46. El Hajal, J.; Thome, J.; Cavallini, A. Condensation in horizontal tubes, part 1: Two-phase flow pattern map. *Int. J. Heat Mass Transf.* **2003**, *46*, 3349–3363. [CrossRef]
47. Schubring, D.; Shedd, T. Critical friction factor modeling of horizontal annular base film thickness. *Int. J. Multiph. Flow* **2009**, *35*, 389–397. [CrossRef]
48. Moreira, T.A.; Colmanetti, A.R.A.; Tibirica, C.B. Heat transfer coefficient: A review of measurement techniques. *J. Braz. Soc. Mech. Sci. Eng.* **2019**, *41*, 264. [CrossRef]
49. Dittus, F.W.; Boelter, L.M.K. Heat transfer in automobile radiators of the tubular type. *Univ. Calif. Pub. Eng.* **1930**, *2*, 443–461. [CrossRef]
50. Moradkhani, M.; Hosseini, S.; Song, M. Robust and general predictive models for condensation heat transfer inside conventional and mini/micro channel heat exchangers. *Appl. Therm. Eng.* **2022**, *201*, 117737. [CrossRef]
51. Akers, W.W.; Deans, H.A.; Crosser, O.K. Condensation Heat Transfer within Horizontal Tubes. *Chem. Eng. Prog. Symp. Ser.* **1958**, *55*, 171–176.
52. Traviss, D.P.; Baron, A.G.; Rohsenow, W.M. Forced-convection condensation inside tubes: A heat transfer equation for condenser design. *ASHRAE Trans.* **1973**, *79*, 157–165.
53. Chang, Y.; Kim, M.; Ro, S. Performance and heat transfer characteristics of hydrocarbon refrigerants in a heat pump system. *Int. J. Refrig.* **2000**, *23*, 232–242. [CrossRef]
54. Bohdal, T.; Charun, H.; Sikora, M. Comparative investigations of the condensation of R134a and R404A refrigerants in pipe minichannels. *Int. J. Heat Mass Transf.* **2011**, *54*, 1963–1974. [CrossRef]

55. Macdonald, M.; Garimella, S. Hydrocarbon condensation in horizontal smooth tubes: Part II–Heat transfer coefficient and pressure drop modeling. *Int. J. Heat Mass Transf.* **2016**, *93*, 1248–1261. [CrossRef]
56. Hosseini, S.; Moradkhani, M.; Valizadeh, M.; Zendehboudi, A.; Olazar, M. A general heat transfer correlation for flow condensation in single port mini and macro channels using genetic programming. *Int. J. Refrig.* **2020**, *119*, 376–389. [CrossRef]
57. Nie, F.; Wang, H.; Zhao, Y.; Song, Q.; Yan, S.; Gong, M. A universal correlation for flow condensation heat transfer in horizontal tubes based on machine learning. *Int. J. Therm. Sci.* **2023**, *184*, 107994. [CrossRef]
58. Zhang, M.; Webb, R.L. Correlation of two-phase friction for refrigerants in small-diameter tubes. *Exp. Therm. Fluid Sci.* **2001**, *25*, 131–139. [CrossRef]
59. Mudawar, I.; Darges, S.J.; Hasan, M.M.; Nahra, H.K.; Balasubramaniam, R.; Mackey, J.R. Experimental investigation and analysis of flow condensation heat transfer in microgravity–Experiments onboard the International Space Station. *Int. J. Heat Mass Transf.* **2026**, *254*, 127602. [CrossRef]

Disclaimer/Publisher's Note: The statements, opinions and data contained in all publications are solely those of the individual author(s) and contributor(s) and not of MDPI and/or the editor(s). MDPI and/or the editor(s) disclaim responsibility for any injury to people or property resulting from any ideas, methods, instructions or products referred to in the content.